Journal of Medicinal Chemistry

Article

Discovery of Small Molecules as Multi-Toll-like Receptor Agonists with Proinflammatory and Anticancer Activities

Lei Zhang, Varun Dewan, and HANG Hubert YIN

J. Med. Chem., **Just Accepted Manuscript** • Publication Date (Web): 24 May 2017

Just Accepted

ACS Publications

Journal of Medicinal Chemistry is published by the American Chemical Society. 1155 Sixteenth Street N.W., Washington, DC 20036

Discovery of Small Molecules as Multi-Toll-like Receptor Agonists with Proinflammatory and Anticancer Activities

Lei Zhang,[1] *Varun Dewan,*[1] *and Hang Yin*[1,*]

[1]Department of Chemistry and Biochemistry and the BioFrontiers Institute, University of Colorado, Boulder, CO 80309, USA

[*]Correspondence: hubert.yin@colorado.edu

KEYWORDS. Toll-like receptor, agonist, high-throughput screening, NF-κB, proinflammatory, anticancer

Abstract. Therapies based on activation of multiple Toll-like receptors (TLRs) may offer superior therapeutic profiles than that of single TLR activation. To discover new small molecules that could activate multiple TLRs, we performed a cell-based high-throughput screening of a small-molecule library based on TLR3-mediated NF-κB activation. Subsequent structural optimization and counter screening of other TLRs produced the first small molecule **17e** (**CU-CPT17e**) capable of simultaneously activating TLRs 3, 8, and 9. Biochemical studies demonstrated that **17e** could induce a strong immune response via the production of various cytokines in human monocytic THP-1 cells. Furthermore, **17e** inhibited the proliferation of HeLa cancer cells by triggering apoptosis and arresting the cell cycle at the S phase. These results showcase potential therapeutic applications of **17e** in both vaccine adjuvants and anticancer therapies based on multi-TLR activation.

Introduction

Toll-like receptors (TLRs) are a family of pattern recognition receptors (PRRs) that play an important role in orchestrating the innate and adaptive immunity to protect the host from invading bacteria, viruses, and other pathogens.[1,2] The activation of different TLRs has also been found to be promising in anticancer therapies.[3-6] With significant therapeutic potential, TLR agonists have been included in the National Cancer Institute's list of immunotherapeutic agents with the highest potential to treat cancer.[7]

Therapies based on multi-TLR activation have considerable benefit over single TLR activation in clinical applications for several reasons. Firstly, multi-TLR activation could augment the immune response by triggering synergism between different TLR pathways.[8-10] Invading pathogens usually release different components which can trigger several TLRs simultaneously in distinct cellular compartments. Instead of working alone, TLRs network with each other to recognize these diverse components of invading pathogens.[11-13] Secondly, polymicrobial infection also occurs when two or more invading microbes are involved at an infection site.[14,15] In these cases, invading microbes are more likely to trigger the activation of several TLRs simultaneously, sometimes even involving other PRRs.[16] The sum of these signals enables the host to mount an effective immune response to clear the invading pathogens. Moreover, the expression of TLRs varies with different tissues and cell types.[17] Even for the same cell type, TLR expression patterns are significantly different from one subpopulation to another. For example, human myeloid dendritic cells (DCs) express TLRs 2 and 4, while plasmacytoid DCs express TLRs 7 and 9.[18] Due to the heterogeneous distribution of TLRs, the efficacy of single TLR activation could diminish or disappear if the target cells fail to express that specific TLR, whereas engagement of multiple TLRs may supplement each other to reach a

critical activation threshold to exert effective immune responses. Therefore, the potential applications of multi-TLR-based therapy in infectious diseases, autoimmune diseases, and cancer have motivated enthusiastic research interest.[19-21]

Numerous reports have shown the promising potential of multi-TLR activation in the development of adjuvant vaccines against infectious and autoimmune diseases.[22-27] For example, the yellow fever vaccine YF-17D, one of the most successful vaccines ever developed, activates TLRs 2, 7, 8, and 9 in dendritic cells to stimulate proinflammatory cytokines.[28,29] In another study of the T-cell response in mice, Berzofsky and coworkers found that a mixture of three TLR ligands (TLR2/6, TLR3, and TLR9) provided more protection against viral infections compared to ligands for only any two of these TLRs.[30]

Different combinations of multiple TLR agonists have also been reported to be more effective in the treatment of various cancers.[19-21] One of the most successful examples is the Bacillus Calmette-Guérin (BCG) vaccine which was originally used against tuberculosis. The BCG vaccine containing components that activate TLRs 2, 4, and 9 has been further successfully developed to treat non-muscle-invasive bladder cancer.[31] In a separate study, the synergistic activity between the TLR3 and TLR9 agonists resulted in an enhanced anti-tumor response, while treatment with either agonist alone failed to control tumor growth.[32,33] Combination therapy by the co-delivery of agonists targeting TLRs 7, 8, and 9 was also reported to eradicate large primary tumors and establish long-term antitumor immunity.[34]

Despite the potential of multi-TLR targeting drugs, most previous reports have been limited to either simply combining several TLR agonists[19-34] or covalently tethering different TLR agonists.[35-39] Moreover, most known TLR agonists are mimics or modifications of microbial

components that have suboptimal pharmacokinetic properties.[40] Small molecules provide an alternative for TLR-based therapeutics. Nonetheless, no small-molecule agonist has been identified for human TLRs 3, 5, or 9.[41] To address these issues, we envisioned that an effective strategy would be to perform a cell-based high-throughput screening (HTS) of small-molecule libraries. In the present study, we chose TLR3 activation as the starting point of our HTS campaign in the hope to extend the activation to other TLRs by further studies. Upon cell-based HTS of a small-molecule library, several hits were identified as TLR3 agonists, among which hit **6a** was chosen in this study based on its potency. Satisfactorily, subsequent structure-activity relationship (SAR) studies and counter screening other TLRs found compound **17e** as the first small-molecule multi-TLR agonist that activates TLRs 3, 8, and 9. The therapeutic potential of **17e** was also investigated in terms of its effect on induction of immune responses and anticancer activities *in vitro*.

Results and discussion

High-throughput screening. The Maybridge HitFinder v11 library comprised of 14,400 compounds was utilized for the cell-based HTS. The human embryonic kidney 293 (HEK293) cell line has been extensively used as a bench-mark expression system for studies involving TLRs.[42] Activation of TLRs upon ligand binding initiates a downstream signaling cascade and results in the activation of transcription factors, such as nuclear factor-κB (NF-κB), eventually leading to the secretion of proinflammatory cytokines and chemokines.[43] Thus, the HEK293 cell line was utilized for the screening system, and was co-transfected with the human TLR3 (hTLR3) gene and an optimized secreted embryonic alkaline phosphatase (SEAP) reporter gene placed under the control of an NF-κB-inducible promoter. The screening layout (**Figure S1A**) was conducted in 384-well plates in duplicate to include controls (basal, positive, and negative)

and library compounds at a final concentration of 30 μM. The efficiency (minimum false positives) and robustness (reproducibility) of the screening procedure was calculated based on the Z' factor,[44] which takes into account the standard deviation and the average values of the positive and the negative controls (**Figure S1B**). The obtained Z' value of our cell-based HTS was 0.77 which was validated to be robust and reliable. TLR3 agonist polyribosinic:polyribocytidic acid (poly I:C) was used as the positive control. SEAP secretion in the cell supernatant was measured to indicate levels of TLR3-mediated NF-κB activation by QUANTI-Blue detection.[45]

Upon successful completion of the HTS, the obtained data was statistically distributed based on the root mean square (RMS) values as depicted in **Figure 1A**. A total of 59 compounds were picked based on activation of the SEAP reporter gene which overlaid most closely to the positive controls (see green highlighted box, **Figure 1A**). To identify exclusive TLR3 activators from the overall hits (NF-κB activators), all identified compounds were then subjected to a second-round manual screening with HEK-null cells which express the NF-κB based SEAP reporter but no TLRs to eliminate generic NF-κB activators. Further rounds of refinement eliminated cytotoxic, non-reproducible and least potent compounds based on EC_{50} calculations from SEAP reporter dose-response studies. From this extensive filtering process, several hits were identified as TLR3 agonists, among which hit compound **6a** (EC_{50} = 22.3 ± 5.3 μM) was picked in this study based on its potency (**Figure 1B**).

Design and Chemistry. With hit **6a** in hand, the structural optimization was performed to target three regions (**Figure 1B**): (a) the substituent effect on the di-benzyl aromatic ring system as well as the difference between di-benzylation and mono-benzylation; (b) replacement of the

ether linkages in the central region; and (c) exploration of other substituted skeletons with a preference for privileged heterocyclic motifs.

Compounds **6a-h**, **9**, and **12** were designed to investigate the SAR of the two phenyl rings at the 6 and 7 positions of the chromene ring (**Scheme 1**). Intermediate **2** was prepared by condensation of 1-(2-hydroxy-4,5-dimethoxyphenyl)ethan-1-one **1** with acetone, which afforded 6,7-dihydroxy-2,2-dimethylchroman-4-one **3** by demethylation with boron tribromide. Due to the electron-withdrawing effect by the carbonyl group, the 7-OH group of compound **3** is more easily ionized. Therefore, methylation or benzylation of compound **3** will selectively occur at the 7-OH group.[46] The intermediate **3** underwent a di-benzylation or methylation/benzylation or mono-benzylation to generate 2,2-dimethylchroman-4-one intermediates **4a-h**, **7**, and **10** respectively, which were then directly reduced by sodium borohydride to give 2,2-dimethylchroman-4-ols **5a-h**, **8**, and **11**. The regioselectivity was further confirmed by the 2D NMR of compound **10**. Target compounds **6a-h**, **9**, and **12** were then obtained through one-step elimination under acidic condition at room temperature.

Looking to replace the dimethyl group on the 2*H*-chromene moiety of **6a** with various substituents, compounds **17a-e** were synthesized using a different route from that of compounds **6a-h** (**Scheme 2**). The synthesis started from condensation of compound **1** with various ketones to afford **13a-f**, which were then demethylated by boron tribromide to give 6,7-dihydroxy-chroman-4-ones **14a-f**. Subsequent reduction of intermediates **14a-f** by lithium aluminium hydride afforded chromane-4,6,7-triols **15a-f**, which were subject to elimination of the hydroxyl group under acidic conditions to give compounds **16a-f**. The final target compounds **17a-e** were conveniently accessed via the di-benzylation of **16a-e** with 4-nitrobenzyl bromide. Compound **18**, a derivative with a different linker than **6a**, was obtained from 2,2-dimethyl-2*H*-chromene-

6,7-diol **16f** via a similar synthetic route, except that a di-benzoylation by 4-nitrobenzoyl chloride was conducted instead of a di-benzylation.

SAR studies. Based on its dose-response results, compound **6a** showed significant NF-κB activation at 25 μM while displaying no cytotoxicity. Therefore, the activation of all the compounds were tested at a concentration of 25 μM in hTLR3 HEK293 cells. Untreated cell samples were used as the baseline control. NF-κB activation of the treated samples was quantified by normalizing to that of the control and expressed as fold changes. Those with NF-κB activation increases of more than 2.5 fold were further tested for their EC_{50} values.

To investigate the role of the two 4-nitrobenzyl groups of **6a**, compounds **12** and **9** were synthesized. There was no TLR3-mediated NF-κB activation observed for any mono-benzylated compounds, highlighting the importance of both 4-nitrobenzyl groups (**Table 1**). Replacing 4-nitrobenzyl groups (**6a**) with 4-nitrobenzoyl groups (**18**) abrogated the activity. Therefore, we maintained the di-benzylated groups on the chromene scaffold of **6a** in the following SAR studies.

Next, we tried to change the substituents on the two symmetric benzyl rings. Absence of the two nitro substituents led to loss of the NF-κB activation (**6a** *vs* **6f**, **Table 2**). No obvious electronic effects on the benzyl rings were observed based on compounds **6b-e**. However, the position of nitro groups played an important role as the meta- and ortho-substituents (**6g** and **6h**) showed no activity compared to their para-substituted counterpart **6a**. Meanwhile, intermediates **4a-e** (chromones) and **5a-e** (chromanols) were also tested. They exhibited similar substituent effects on the benzyl groups as that of compounds **6a-e**. On the other hand, the chromene

scaffold was the most potent activator of TLR3-mediated NF-κB signaling as compared to chromone and chromanol scaffolds, exemplified by compounds **6a**, **4a**, and **5a**.

Optimization studies were then directed to examine different substituted chromene scaffolds (**Table 3**). Chromenes with 2,2-diethyl (**17a**), cyclohexane (**17b**), cyclopentane (**17c**), cycloheptane (**17d**) substituents displayed no NF-κB activation. However, tetrahydro-2*H*-pyran substitution (**17e**) significantly improved the activity with 13.9 ± 0.9 fold of NF-κB activation and an EC_{50} value of 4.8 ± 0.7 μM. Therefore, compound **17e** (**CU-CPT17e**) was identified as the best derivative for subsequent biological evaluations.[47]

Compound 17e is a multi-TLR agonist that activates TLRs 3, 8, and 9. We were interested to see whether **17e** could activate NF-κB by tapping other hTLR signaling pathways. To this end, the best derivative **17e** was tested by the SEAP assay using HEK293 cells transfected with various hTLRs. As shown in **Figure 2**, compound **17e** showed negligible or no NF-κB activation in hTLRs 2, 4, 5, and 7 cells compared with the activation by the cognate agonists of these TLRs. Nonetheless, compound **17e** showed strong NF-κB activation in TLR8 and TLR9 cells with EC_{50} values of 13.5 ± 0.6 μM and 5.7 ± 0.2 μM respectively (**Table 4**). These results indicated that **17e** is a novel small-molecule TLR3/8/9 agonist.

The therapeutic potential of **17e** was further explored in a bifurcate manner: its effect on induction of immune response and anticancer activities *in vitro*.

Compound 17e stimulates cytokine responses in THP-1 cells. As a response to harmful stimuli, immune cells stimulated via TLR activation release various cytokines to activate other immune cells to cope with invading pathogens or deleterious tissue damages.[1,2] Human monocytic THP-1 cells express TLRs 1-10 and are widely used as a model system to study Toll-

like receptors.[48] To characterize its immunostimulatory activity, compound **17e** was tested in THP-1 cells along with several standards such as poly I:C (TLR3 agonist), R848 (TLR7/8 agonist), and CpG ODN2006 (TLR9 agonist). Levels of cytokine tumor necrosis factor α (TNF-α) from cell culture supernatants were analyzed by the enzyme-linked immunosorbent assay (ELISA). As shown in **Figure 3A**, compound **17e** stimulated a strong production of TNF-α in THP-1 cells in a dose-dependent manner. Additionally, the effect of **17e** on mRNA expression of various proinflammatory cytokines was also examined by qRT-PCR. The results showed that the mRNA levels of TNF-α (**Figure 3B**), interleukin 6 (IL-6) (**Figure 3C**), and IL-8 (**Figure 3D**) significantly increased after 12 hours in a dose-dependent manner. Collectively, our data suggested that **17e** could induce strong proinflammatory signals at both transcriptional and translational levels in human monocytic THP-1 cells.

Compound 17e inhibits the proliferation of cancer cells in a dose-dependent manner. The antitumor role of TLR-based therapies has been attributed to the enhancement of innate and adaptive immunity, interference with cell cycle regulation, or a direct proapoptotic effect on tumor cells.[49-51] To investigate its effects on tumor cells, compound **17e** was evaluated for the antiproliferative property in several human cancer cell lines including HeLa, MDA-MB-231, VA-13, U-2 OS, SCaBER, and MCF-7 cells. Among those, the HeLa cell line was found particularly sensitive to **17e**, which may be caused by varied expression patterns and amounts of TLRs in different cancer cell lines.[3-6] Therefore, HeLa cells were selected for further investigation. The antiproliferative effect of **17e** on human HeLa cells was examined by the WST-1 assay. As shown in **Figure 4A**, following exposure to **17e** for 24, 48, and 72 hours, the proliferation of the HeLa cell line was strongly inhibited in a dose-dependent manner. To determine the degree of toxicity of **17e** towards normal cells, parallel experiments were

conducted in normal human mammary epithelial cells (HuMEC). Compound **17e** showed only mild cytotoxicity to HuMEC cells (**Figure 4B** and **Table 5**).

Compound 17e triggers apoptosis in HeLa cells. To gain insights into the underlying mechanism for cell growth inhibition by **17e**, we further investigated the induction of apoptosis by **17e** in HeLa cells. HeLa cells were cultured with increasing concentrations of **17e** or poly I:C or blank control (DMSO) for 24 hours. Induction of apoptosis was monitored by flow cytometry using annexin V and propidium iodide (PI) double staining, which detects the externalization of phosphatidylserine (PS), a characteristic feature of cells entering apoptosis.[52] The phospholipid-binding protein, annexin V, binds to cells with externally exposed PS, while PI staining occurs only after loss of membrane integrity.[53] This dual staining distinguishes between unaffected cells (Q4, Annexin V^-/PI^-), early apoptotic cells (Q3, Annexin V^+/PI^-), late apoptotic cells (Q2, Annexin V^+/PI^+), and necrotic cells (Q1, Annexin V^-/PI^+). As shown in **Figure 5**, treatment with **17e** for 24 hours at different concentrations (10 to 40 μM) resulted in an elevation of apoptotic cell population ranging from 10% to 17% (**Figures 5C-F**), which is more effective than poly I:C at 5 μg/mL (**Figure 5G**). These results suggested that the antiproliferative activity of **17e** against HeLa cells might result from its ability to directly induce apoptosis.

Compound 17e arrests the cell cycle at the S phase in HeLa cells. To delineate the mechanism behind apoptosis, the effect of **17e** on the cell cycle distribution of HeLa cells was also examined by staining cells with PI and analyzing the percentages of G0/G1, S, and G2/M cell populations with flow cytometry. As shown in **Figure 6G**, treatment with **17e** for 24 hours caused a dose-dependent accumulation of cells at the S phase accompanied with a reduction of G0/G1 cells. Specifically, the percentage of cells at the G0/G1 phase was about 52% in the control group, but gradually decreased to 40% after treatment with different concentrations of

17e. In addition, the percentage of cells at the S phase increased from 31% in the control group to 41% after treatment with **17e**. The arrest of the cell cycle at the S phase could block DNA synthesis and cause DNA damage. Cells are prone to undergo apoptosis when damage repair is impeded or incomplete. Taken together, these results indicate that **17e** arrested HeLa cells at the S phase, leading to the apoptosis.

Modulation of several targets by a single agent can provide a superior safety and efficacy profile due to lower dosages and thus less side effects and drug resistance.[54-56] This is especially beneficial to complex diseases including many infectious and autoimmune diseases as well as cancer.[57-59] However, studies of single agents that activate multiple TLRs are still rare.[35-39] In this study, we successfully identified the first small molecule TLR3/8/9 agonist **17e** from a cell-based HTS campaign and subsequent structural optimizations. Although the molecular mechanisms by which **17e** activates TLRs 3, 8, and 9 remains elusive, some speculations can be drawn based on the structural and functional similarities between them. TLRs 3, 8, and 9 are highly homologous and all confined to the membranes of endosomes to recognize nucleic acids (RNA or DNA).[60,61] It is also interesting that **17e** selectively activates TLR8 over TLR7, both of which recognize ssRNA within the endosomes. This may be due to its different binding affinity or even distinct binding pockets to TLR7 and TLR8.[62] Some reports have found that activation of TLRs 7 and/or 8 is very sensitive to structural modifications of the agonists.[63-65] For example, imidazoquinolines with a butyl group activated TLR7, but simply replacing with a pentyl group caused specific TLR8 activation.[66] Understanding the molecular basis of the multi-TLR agonist **17e** will facilitate its further development in multi-TLR based therapies as well as help the studies of TLR biology.

Proinflammatory assays showed that **17e** induced large amounts of cytokines such as TNF-α, IL-6, and IL-8 in THP-1 cells at both transcriptional and translational levels. A strong inflammatory response might suggest a long duration of immune response and full deployment of immune cells. This brings more clinical benefit particularly to newborns[67] and the elderly[68] who generally suffer from poor immunogenicity. Moreover, compound **17e** can inhibit the growth of human cervical HeLa cancer cells by inducing apoptosis and arresting the cell cycle at the S phase. Regulation of the cell cycle and apoptosis can be important targets for cancer chemotherapy.[69] The mechanism underlying the anti-tumor property of **17e** will be examined latter by analyzing the changes of cell cycle markers, death receptors, caspases and alike. These results suggest promising therapeutic applications of **17e** in the development of vaccine adjuvants and anticancer therapies.

Conclusion

In summary, we utilized a cell-based high-throughput screening to assist in the discovery of small-molecule multi-TLR agonists. The strategy was to initially focus on TLR3 activation in the HTS and SAR studies, then extend to other TLRs, eventually leading to the discovery of compound **17e** as a potent multi-TLR agonist which activates TLRs 3, 8, and 9. Proinflammatory studies proved that **17e** can induce a robust immune response via the production of various cytokines in human monocytic THP-1 cells at both mRNA and protein levels. **17e** can also cause growth inhibition, apoptosis induction, and cell cycle arrest in human cervical cancer cells. This work expands the limited repertoire of available small-molecule TLR agonists and warrants in-depth investigations to explore the potential therapeutic applications in vaccine adjuvants and anticancer therapies.

Experimental

General Chemistry Methods. Reagents were purchased from commercial sources and used as received. ^{1}H NMR spectra were recorded at 400 MHz in $CDCl_3$ or CD_3OD using residual solvent peaks ($CDCl_3$: δ 7.28; CD_3OD: δ 3.30) as the internal standard. ^{13}C NMR spectra were recorded at 101 MHz in $CDCl_3$ using residual $CHCl_3$ (77.16 ppm) as the internal reference. Compounds were purified using flash chromatography (ACI systems, Biotage). The purity of tested compounds was evaluated via ^{1}H NMR (>95% sample purity). Mass spectrometry was performed at the mass spectrometry facility of the Department of Chemistry at the University of Colorado at Boulder on a double focusing high resolution mass spectrometer.

Synthesis of 6,7-Dimethoxy-2,2-dimethyl-3*H*-1-benzopyran-4-one (2). To a solution of 1-(2-hydroxy-4,5-dimethoxyphenyl)ethan-1-one **1** (5 g, 25.48 mmol) in methanol, pyrrolidine (4.2 mL, 50.97 mmol) and acetone (20 ml, 272.04 mmol) were added sequentially and the reaction mixture was heated to reflux overnight before concentrating and purifying by flash column chromatography to give the title compound **2** (5.12 g, 85%) as a white solid. ^{1}H NMR (400 MHz, $CDCl_3$) δ 7.28 (s, 1H), 6.42 (s, 1H), 3.92 (s, 3H), 3.89 (s, 3H), 2.68 (s, 2H), 1.47 (s, 6H); MS (ESI^+) m/z 237.1 $[M+H]^+$.

Synthesis of 6,7-Dihydroxy-2,2-dimethylchroman-4-one (3). To a solution of **2** (5 g, 21.16 mmol) in dichloromethane (20 mL) was slowly added boron tribromide (1M in dichloromethane, 63.49 mL, 63.49 mmol) at 0 ^{o}C under nitrogen and the reaction was stirred at room temperature overnight. The reaction mixture was poured into ice water, extracted with ethyl acetate for three times. The combined organic layers were dried with Na_2SO_4, filtered, concentrated, and purified by flash column chromatography to give the title compound **3** (3.53 g, 80%) as a white solid. ^{1}H

NMR (400 MHz, CD_3OD) δ 7.14 (s, 1H), 6.30 (s, 1H), 4.95 (br s, 2H), 2.61 (s, 2H), 1.39 (s, 6H); MS (ESI^+) m/z 209.1 $[M+H]^+$.

General Procedure for the Preparation of Compounds 4a-e Exemplified by 2,2-Dimethyl-6,7-bis((4-nitrobenzyl)oxy)chroman-4-one (4a). A mixture of **3** (300 mg, 1.44 mmol) and potassium carbonate (1.19 g, 8.64 mmol) in acetone (20 mL) was treated with 4-nitrobenzyl bromide (685 mg, 3.17 mmol) and stirred at 60 ^oC under nitrogen overnight. The reaction mixture was filtered, concentrated, and purified by flash column chromatography to give the title compound **4a** (648 mg, 94%) as a yellow solid. ^1H NMR (400 MHz, $CDCl_3$) δ 8.28 (dd, J = 11.1, 8.8 Hz, 4H), 7.64 (dd, J = 8.9, 2.2 Hz, 4H), 7.39 (s, 1H), 6.46 (s, 1H), 5.29 (s, 2H), 5.24 (s, 2H), 2.68 (s, 2H), 1.46 (s, 6H); ^{13}C NMR (101 MHz, $CDCl_3$) δ 190.83, 156.64, 155.16, 147.81, 147.63, 144.18, 143.15, 142.73, 127.50, 127.39, 124.00, 123.84, 113.12, 109.91, 102.53, 79.90, 70.05, 69.43, 48.34, 26.60; HRMS (ESI^+), calcd $C_{25}H_{22}LiN_2O_8$ ($M + Li^+$) = 485.1536, found = 485.1544.

2,2-Dimethyl-6,7-bis((4-(trifluoromethyl)benzyl)oxy)chroman-4-one (4b). White solid, yield 92%. ^1H NMR (400 MHz, $CDCl_3$) δ 7.65 (dd, J = 12.0, 8.2 Hz, 4H), 7.57 (dd, J = 8.1, 4.2 Hz, 4H), 7.41 (s, 1H), 6.47 (s, 1H), 5.22 (s, 2H), 5.17 (s, 2H), 2.67 (s, 2H), 1.46 (s, 6H); 13C NMR (101 MHz, CDCl3) δ 190.88, 156.63, 155.64, 143.04, 140.95, 139.99, 127.27, 127.09, 125.69, 125.66, 125.62, 125.58, 125.51, 125.47, 125.44, 125.40, 125.36, 112.98, 110.08, 102.45, 79.76, 70.58, 69.81, 48.35, 26.56; HRMS (ESI^+), calcd $C_{27}H_{22}F_6LiO_4$ ($M + Li^+$) = 531.1582, found = 531.1577.

6,7-Bis((3-fluoro-4-nitrobenzyl)oxy)-2,2-dimethylchroman-4-one (4c). Yellow solid, yield 87%. ^1H NMR (400 MHz, $CDCl_3$) δ 8.08–8.00 (m, 2H), 7.40–7.33 (m, 2H), 7.31–7.28 (m, 2H),

7.19 (s, 1H), 6.35 (s, 1H), 5.16 (s, 2H), 5.12 (s, 2H), 2.60 (s, 2H), 1.37 (s, 6H); ^{13}C NMR (101 MHz, $CDCl_3$) δ 190.77, 157.11, 156.70, 154.71, 154.47, 146.04, 145.96, 144.93, 144.85, 142.42, 126.70, 126.68, 126.51, 126.48, 122.27, 122.23, 122.19, 122.15, 116.50, 116.28, 113.29, 109.84, 102.59, 80.02, 69.30, 68.74, 48.32, 26.64, 26.59; HRMS (ESI^+), calcd $C_{25}H_{20}F_2LiN_2O_8$ ($M + Li^+$) = 521.1348, found = 521.1359.

6,7-Bis((3,4-difluorobenzyl)oxy)-2,2-dimethylchroman-4-one (4d). White solid, yield 85%. ^{1}H NMR (400 MHz, $CDCl_3$) δ 7.35 (s, 1H), 7.30–7.24 (m, 2H), 7.19–7.11 (m, 4H), 6.43 (s, 1H), 5.07 (s, 2H), 5.02 (s, 2H), 2.65 (s, 2H), 1.44 (s, 6H); ^{13}C NMR (101 MHz, $CDCl_3$) δ 190.85, 156.63, 155.58, 151.74, 151.66, 151.62, 151.53, 151.38, 151.26, 151.21, 151.09, 149.27, 149.19, 149.14, 149.06, 148.91, 148.79, 148.75, 148.62, 142.90, 134.01, 133.96, 133.92, 133.02, 132.96, 132.92, 123.20, 123.17, 123.14, 123.12, 123.10, 123.09, 123.06, 123.02, 117.59, 117.42, 117.34, 117.16, 116.36, 116.29, 116.18, 116.11, 112.93, 110.15, 102.41, 79.73, 70.17, 69.37, 48.32, 26.53; HRMS (ESI+), calcd $C_{25}H_{20}F_4LiO_4$ ($M + Li^+$) = 467.1458, found = 467.1453.

6,7-Bis((3-fluoro-4-methoxybenzyl)oxy)-2,2-dimethylchroman-4-one (4e). White solid, yield 83%. ^{1}H NMR (400 MHz, $CDCl_3$) δ 7.38 (s, 1H), 7.21–7.13 (m, 4H), 7.01–6.93 (m, 2H), 6.44 (s, 1H), 5.07 (s, 2H), 5.02 (s, 2H), 3.92 (s, 3H), 3.90 (s, 3H), 2.66 (s, 2H), 1.45 (s, 6H); ^{13}C NMR (101 MHz, $CDCl_3$) δ 190.95, 156.57, 156.05, 153.60, 153.57, 151.15, 151.12, 147.62, 147.51, 147.39, 147.28, 143.15, 129.94, 129.88, 128.87, 128.81, 123.40, 123.37, 123.25, 123.22, 115.53, 115.38, 115.34, 115.19, 113.40, 113.20, 112.78, 110.42, 102.41, 79.63, 70.76, 69.91, 56.29, 56.27, 48.41, 26.63; HRMS (ESI+), calcd $C_{27}H_{26}F_2LiO_6$ ($M + Li^+$) = 491.1857, found = 491.1855.

General Procedure for the Preparation of Compounds 5a-e Exemplified by 2,2-Dimethyl-6,7-bis((4-nitrobenzyl)oxy)chroman-4-ol (5a). A mixture of **4a** (400 mg, 0.84 mmol) and sodium borohydride (64 mg, 1.67 mmol) in absolute methanol (20 mL) was stirred at 60 ^{o}C. After 3 h, the solution was poured into water and extracted with ethyl acetate. The organic phase was dried with Na_2SO_4, filtered, concentrated, and purified by flash column chromatography to afford the title compound **5a** (325 mg, 81%) as a yellow solid. ^{1}H NMR (400 MHz, $CDCl_3$) δ 8.27–8.19 (m, 4H), 7.66–7.59 (m, 4H), 7.08 (s, 1H), 6.40 (s, 1H), 5.21 (s, 2H), 5.21 (s, 2H), 4.77 (dd, J = 14.3, 7.8 Hz, 1H), 2.17 (dd, J = 13.4, 6.1 Hz, 1H), 1.83 (dd, J = 13.4, 8.7 Hz, 1H), 1.70 (d, J = 7.4 Hz, 1H), 1.43 (s, 3H), 1.30 (s, 3H); ^{13}C NMR (101 MHz, $CDCl_3$) δ 149.36, 148.48, 147.59, 147.52, 144.92, 144.25, 142.09, 127.57, 127.40, 123.85, 123.75, 116.55, 114.69, 103.30, 75.66, 71.06, 69.58, 63.49, 42.91, 28.80, 25.71; HRMS (ESI$^+$), calcd $C_{25}H_{24}LiN_2O_8$ (M + Li^+) = 487.1693, found = 487.1692.

2,2-Dimethyl-6,7-bis((4-(trifluoromethyl)benzyl)oxy)chroman-4-ol (5b). White solid, yield 98%. ^{1}H NMR (400 MHz, $CDCl_3$) δ 7.65–7.60 (m, 4H), 7.55 (dd, J = 8.1, 2.9 Hz, 4H), 7.09 (s, 1H), 6.43 (s, 1H), 5.13 (s, 2H), 5.10 (s, 2H), 4.74 (dd, J = 14.1, 7.1 Hz, 1H), 2.15 (d, J = 4.8 Hz, 1H), 2.12 (dd, J = 12.5, 5.2 Hz, 1H), 1.79 (dd, J = 13.4, 8.8 Hz, 1H), 1.42 (s, 3H), 1.30 (s, 3H); ^{13}C NMR (101 MHz, $CDCl_3$) δ 149.79, 148.43, 142.36, 141.57, 140.95, 127.42, 127.18, 125.53, 125.49, 125.45, 125.41, 125.37, 125.33, 125.30, 116.42, 115.04, 103.28, 75.60, 71.67, 69.97, 63.44, 42.83, 28.81, 25.55; HRMS (ESI$^+$), calcd $C_{27}H_{24}F_6LiO_4$ (M + Li^+) = 533.1739, found = 533.1743.

6,7-Bis((3-fluoro-4-nitrobenzyl)oxy)-2,2-dimethylchroman-4-ol (5c). Yellow solid, yield 88%. ^{1}H NMR (400 MHz, $CDCl_3$) δ 8.12–8.08 (m, 2H), 7.47–7.35 (m, 4H), 7.08 (s, 1H), 6.37 (s, 1H), 5.18 (s, 4H), 4.81–4.76 (m, 1H), 2.18 (dd, J = 13.4, 6.1 Hz, 1H), 1.86–1.80 (m, 1H), 1.71

(d, J = 7.6 Hz, 1H), 1.44 (s, 3H), 1.31 (s, 3H); ^{13}C NMR (101 MHz, $CDCl_3$) δ 157.09, 154.45, 148.97, 148.63, 146.86, 146.78, 146.14, 146.06, 141.79, 126.51, 126.49, 126.38, 126.36, 122.33, 122.29, 122.21, 122.17, 116.85, 116.57, 116.46, 116.35, 116.24, 114.60, 103.29, 75.76, 70.34, 68.93, 63.43, 42.88, 28.82, 25.67; HRMS (ESI^+), calcd $C_{25}H_{22}F_2LiN_2O_8$ ($M + Li^+$) = 523.1504, found = 523.1508.

6,7-Bis((3,4-difluorobenzyl)oxy)-2,2-dimethylchroman-4-ol (5d). White solid, yield 75%. ^{1}H NMR (400 MHz, $CDCl_3$) δ 7.28–7.23 (m, 2H), 7.16–7.08 (m, 4H), 7.04 (s, 1H), 6.39 (s, 1H), 4.98 (s, 2H), 4.94 (s, 2H), 4.70 (dd, J = 14.1, 7.0 Hz, 1H), 2.47 (d, J = 6.8 Hz, 1H), 2.09 (dd, J = 13.4, 6.2 Hz, 1H), 1.76 (dd, J = 13.4, 8.9 Hz, 1H), 1.41 (s, 3H), 1.28 (s, 3H); ^{13}C NMR (101 MHz, $CDCl_3$) δ 151.67, 151.59, 151.54, 151.46, 151.23, 151.16, 151.10, 151.04, 149.68, 149.20, 149.12, 149.07, 148.99, 148.76, 148.70, 148.63, 148.58, 148.43, 142.19, 134.61, 134.56, 134.52, 133.98, 133.93, 133.89, 123.39, 123.36, 123.33, 123.30, 123.19, 123.15, 123.13, 123.09, 117.39, 117.22, 117.04, 116.56, 116.46, 116.39, 116.34, 116.16, 115.16, 103.24, 75.62, 71.28, 69.54, 63.34, 42.75, 28.84, 25.48; HRMS (ESI^+), calcd $C_{25}H_{22}F_4LiO_4$ ($M + Li^+$) = 469.1614, found = 469.1612.

6,7-Bis((3-fluoro-4-methoxybenzyl)oxy)-2,2-dimethylchroman-4-ol (5e). White solid, yield 71%. ^{1}H NMR (400 MHz, $CDCl_3$) δ 7.20–7.10 (m, 4H), 7.03 (s, 1H), 6.96–6.89 (m, 2H), 6.40 (s, 1H), 4.97 (s, 2H), 4.93 (s, 2H), 4.74–4.67 (m, 1H), 3.88 (s, 3H), 3.87 (s, 3H), 2.14 (d, J = 5.7 Hz, 1H), 2.09 (dd, J = 13.4, 6.1 Hz, 1H), 1.77 (dd, J = 13.4, 8.7 Hz, 1H), 1.40 (s, 3H), 1.28 (s, 3H); ^{13}C NMR (101 MHz, $CDCl_3$) δ 153.53, 153.46, 151.08, 151.02, 150.02, 148.24, 147.34, 147.26, 147.24, 147.15, 142.47, 130.59, 130.53, 129.95, 129.89, 123.57, 123.54, 123.33, 123.30, 116.17, 115.71, 115.52, 115.46, 115.27, 115.25, 113.29, 113.13, 103.33, 75.45, 71.75, 70.02, 63.43,

56.26, 56.23, 42.80, 28.81, 25.69; HRMS (ESI^+), calcd $C_{27}H_{28}F_2LiO_6$ ($M + Li^+$) = 493.2014, found = 493.2016.

General Procedure for the Preparation of Compounds 6a-h Exemplified by 2,2-Dimethyl-6,7-bis((4-nitrobenzyl)oxy)-2*H*-chromene (6a). Compound **5a** (200 mg, 0.42 mmol) was dissolved in acetone (10 mL) and then 4 N HCl (0.8 mL) was added. The reaction mixture was stirred overnight at room temperature. The reaction was basified with saturated $NaHCO_3$ solution and extracted with ethyl acetate. The combined organic layers were dried with Na_2SO_4, filtered, concentrated, and purified by flash column chromatography to afford the title compound **6a** (184 mg, 96%) as a yellow solid. ^1H NMR (400 MHz, $CDCl_3$) δ 8.25 (dd, J = 8.3, 3.1 Hz, 4H), 7.62 (dd, J = 8.3, 3.1 Hz, 4H), 6.62 (s, 1H), 6.45 (s, 1H), 6.21 (d, J = 9.7 Hz, 1H), 5.53 (d, J = 9.7 Hz, 1H), 5.22 (s, 2H), 5.19 (s, 2H), 1.42 (s, 6H); ^{13}C NMR (101 MHz, $CDCl_3$) δ 149.12, 148.44, 147.61, 147.54, 144.93, 144.23, 141.98, 129.19, 127.59, 127.44, 123.85, 123.75, 121.48, 114.61, 114.35, 103.50, 76.35, 71.41, 69.76, 29.72, 27.76; HRMS (ESI^+), calcd $C_{25}H_{22}LiN_2O_7$ ($M + Li^+$) = 469.1587, found = 469.1594.

2,2-Dimethyl-6,7-bis((4-(trifluoromethyl)benzyl)oxy)-2*H*-chromene (6b). White solid, yield 97%. ^1H NMR (400 MHz, $CDCl_3$) δ 7.67–7.61 (m, 4H), 7.55 (d, J = 8.1 Hz, 4H), 6.65 (s, 1H), 6.48 (s, 1H), 6.22 (d, J = 9.7 Hz, 1H), 5.53 (d, J = 9.7 Hz, 1H), 5.17 (s, 2H), 5.13 (s, 2H), 1.43 (s, 6H); ^{13}C NMR (101 MHz, $CDCl_3$) δ 149.58, 148.34, 142.33, 141.63, 140.95, 128.92, 127.38, 127.22, 125.43 (dq, J = 10.9, 3.8 Hz), 121.65, 114.60, 114.40, 103.56, 76.24, 71.98, 70.20, 27.74; HRMS (ESI^+), calcd $C_{27}H_{22}F_6LiO_3$ ($M + Li^+$) = 515.1633, found = 515.1635.

6,7-Bis((3-fluoro-4-nitrobenzyl)oxy)-2,2-dimethyl-2*H*-chromene (6c). Yellow solid, yield 90%. ^1H NMR (400 MHz, $CDCl_3$) δ 8.13–8.08 (m, 2H), 7.47–7.39 (m, 2H), 7.37–7.34 (m, 2H),

6.62 (s, 1H), 6.43 (s, 1H), 6.21 (d, J = 9.7 Hz, 1H), 5.55 (d, J = 9.7 Hz, 1H), 5.19 (s, 2H), 5.15 (s, 2H), 1.42 (s, 6H); ^{13}C NMR (101 MHz, $CDCl_3$) δ 157.08, 154.39, 148.75, 148.61, 146.84, 146.76, 146.10, 146.02, 141.74, 129.43, 126.50, 126.47, 126.38, 126.35, 122.32, 122.28, 122.25, 122.21, 121.35, 116.59, 116.50, 116.37, 116.29, 114.88, 114.24, 103.51, 76.44, 70.73, 69.15, 27.78; HRMS (ESI$^+$), calcd $C_{25}H_{20}F_2LiN_2O_7$ (M + Li^+) = 505.1399, found = 505.1407.

6,7-Bis((3,4-difluorobenzyl)oxy)-2,2-dimethyl-2*H*-chromene (6d). White solid, yield 90%. ^{1}H NMR (400 MHz, $CDCl_3$) δ 7.29 (dt, J = 16.5, 5.3 Hz, 2H), 7.19–7.11 (m, 4H), 6.64 (s, 1H), 6.48 (s, 1H), 6.23 (d, J = 9.7 Hz, 1H), 5.53 (d, J = 9.7 Hz, 1H), 5.03 (s, 2H), 4.99 (s, 2H), 1.44 (s, 6H); ^{13}C NMR (101 MHz, $CDCl_3$) δ 151.61 (dd, J = 12.7, 6.2 Hz), 151.18 (dd, J = 12.6, 7.4 Hz), 149.56, 149.14 (dd, J = 12.7, 6.0 Hz), 148.71 (dd, J = 12.6, 7.1 Hz), 148.39, 142.25, 134.66 (dd, J = 5.3, 4.0 Hz), 133.98 (dd, J = 5.4, 4.0 Hz), 128.93, 123.25 (ddd, J = 12.3, 6.4, 3.7 Hz), 121.66, 117.48–117.00 (m), 116.40 (dd, J = 17.7, 15.5 Hz), 114.70, 114.43, 103.59, 76.23, 71.57, 69.79, 27.73; HRMS (ESI$^+$), calcd $C_{25}H_{20}F_4LiO_3$ (M + Li^+) = 451.1509, found = 451.1508.

6,7-Bis((3-fluoro-4-methoxybenzyl)oxy)-2,2-dimethyl-2*H*-chromene (6e). White solid, yield 88%. ^{1}H NMR (400 MHz, $CDCl_3$) δ 7.24–7.07 (m, 4H), 6.94 (dt, J = 10.9, 8.5 Hz, 2H), 6.62 (s, 1H), 6.47 (s, 1H), 6.21 (d, J = 9.7 Hz, 1H), 5.50 (d, J = 9.7 Hz, 1H), 5.01 (s, 2H), 4.96 (s, 2H), 3.90 (s, 3H), 3.89 (s, 3H), 1.42 (s, 6H); ^{13}C NMR (101 MHz, $CDCl_3$) δ 153.56, 153.50, 151.12, 151.06, 149.93, 148.22, 147.40, 147.30, 147.19, 142.46, 130.68, 130.62, 129.97, 129.91, 128.66, 123.54, 123.51, 123.39, 123.36, 121.81, 115.71, 115.52, 115.34, 114.96, 114.16, 113.30, 113.16, 103.65, 76.12, 72.07, 70.24, 56.27, 56.25, 27.76; HRMS (ESI+), calcd $C_{27}H_{26}F_2LiO_5$ (M + Li^+) = 475.1908, found = 475.1909.

6,7-Bis(benzyloxy)-2,2-dimethyl-2*H*-chromene (6f). White solid, yield 97%. ^{1}H NMR (400 MHz, $CDCl_3$) δ 7.53–7.45 (m, 4H), 7.45–7.32 (m, 6H), 6.68 (s, 1H), 6.55 (s, 1H), 6.25 (d, J = 9.7 Hz, 1H), 5.52 (d, J = 9.7 Hz, 1H), 5.16 (s, 2H), 5.11 (s, 2H), 1.46 (s, 6H). ^{13}C NMR (101 MHz, $CDCl_3$) δ 150.23, 148.15, 142.76, 137.75, 137.09, 128.51, 128.42, 127.84, 127.75, 127.61, 127.35, 121.95, 114.93, 114.01, 103.64, 76.09, 72.94, 71.05, 27.81; HRMS (ESI^+), calcd $C_{25}H_{24}LiO_3$ ($M + Li^+$) = 379.1885, found = 379.1885.

2,2-Dimethyl-6,7-bis((3-nitrobenzyl)oxy)-2*H*-chromene (6g). Yellow solid, yield 95%. ^{1}H NMR (400 MHz, $CDCl_3$) δ 8.34 (d, J = 1.8 Hz, 2H), 8.21–8.13 (m, 2H), 7.85–7.76 (m, 2H), 7.57 (dd, J = 15.4, 7.6 Hz, 2H), 6.68 (s, 1H), 6.50 (s, 1H), 6.24 (d, J = 9.7 Hz, 1H), 5.54 (d, J = 9.7 Hz, 1H), 5.19 (s, 2H), 5.16 (s, 2H), 1.43 (s, 6H); 13C NMR (101 MHz, CDCl3) δ 149.21, 148.45, 148.39, 148.33, 142.06, 139.63, 139.00, 133.14, 132.97, 129.64, 129.52, 129.13, 122.93, 122.79, 122.09, 121.92, 121.56, 114.60, 114.32, 103.47, 76.33, 71.32, 69.65, 27.76; HRMS (ESI^+), calcd $C_{25}H_{22}LiN_2O_7$ ($M + Li^+$) = 469.1587, found = 469.1584.

2,2-Dimethyl-6,7-bis((2-nitrobenzyl)oxy)-2*H*-chromene (6h). Yellow solid, yield 87%. ^{1}H NMR (400 MHz, $CDCl_3$) δ 8.23–8.15 (m, 2H), 8.05 (dd, J = 7.9, 1.0 Hz, 1H), 7.94 (dd, J = 7.9, 1.0 Hz, 1H), 7.73–7.64 (m, 2H), 7.53–7.47 (m, 2H), 6.69 (s, 1H), 6.51 (s, 1H), 6.25 (d, J = 9.7 Hz, 1H), 5.55 (s, 2H), 5.52 (d, J = 9.7 Hz, 1H), 5.51 (s, 2H), 1.43 (s, 6H); ^{13}C NMR (101 MHz, $CDCl_3$) δ 149.06, 148.33, 146.86, 146.75, 142.06, 134.46, 134.04, 133.95, 133.86, 129.03, 128.75, 128.49, 128.31, 128.21, 125.01, 124.85, 121.62, 114.52, 113.89, 103.44, 76.30, 69.26, 67.94, 27.76; HRMS (ESI^+), calcd $C_{25}H_{22}LiN_2O_7$ ($M + Li^+$) = 469.1587, found = 469.1582.

7-Methoxy-2,2-dimethyl-6-((4-nitrobenzyl)oxy)chroman-4-one (7). To a solution of **3** (400 mg, 1.92 mmol) and potassium carbonate (292 mg, 2.11 mmol) in *N*,*N*-dimethylformamide (20

mL) was added methyl iodide (0.12 ml, 1.92 mmol). The reaction mixture was stirred at 80 ^{o}C for 8 h. When the reaction was completed, the mixture was cooled to room temperature, and then 4-nitrobenzyl bromide (415 mg, 1.92 mmol) and potassium carbonate (292 mg, 2.11 mmol) was added. The resultant mixture was stirred at room temperature overnight. The solution was poured into water and extracted with ethyl acetate. The organic phase was dried with Na_2SO_4, filtered, concentrated, and purified by flash column chromatography to afford the title compound **7** (617 mg, 90%) as a yellow solid. ^{1}H NMR (400 MHz, $CDCl_3$) δ 8.22 (d, J = 8.8 Hz, 2H), 7.61 (d, J = 8.9 Hz, 2H), 7.29 (s, 1H), 6.43 (s, 1H), 5.18 (s, 2H), 3.91 (s, 3H), 2.64 (s, 2H), 1.44 (s, 6H); ^{13}C NMR (101 MHz, $CDCl_3$) δ 190.80, 156.94, 156.90, 147.54, 144.28, 142.47, 127.63, 123.77, 112.29, 109.29, 100.95, 79.71, 69.96, 56.22, 48.31, 26.60; HRMS (ESI^+), calcd $C_{19}H_{19}LiNO_6$ (M + Li^+) = 364.1372, found = 364.1370.

Synthesis of 7-Methoxy-2,2-dimethyl-6-((4-nitrobenzyl)oxy)chroman-4-ol (8). A mixture of **7** (400 mg, 1.12 mmol) and sodium borohydride (85 mg, 2.24 mmol) in absolute methanol (20 mL) was stirred at 60 ^{o}C. After 3 h, the solution was poured into water and extracted with ethyl acetate. The organic phase was dried with Na_2SO_4, filtered, concentrated, and purified by flash column chromatography to afford the title compound **8** (350 mg, 87%) as a yellow solid. ^{1}H NMR (400 MHz, $CDCl_3$) δ 8.17 (d, J = 8.8 Hz, 2H), 7.58 (d, J = 8.8 Hz, 2H), 6.96 (s, 1H), 6.35 (s, 1H), 5.09 (s, 2H), 4.68 (dd, J = 14.3, 7.1 Hz, 1H), 3.80 (s, 3H), 2.31 (d, J = 7.0 Hz, 1H), 2.07 (dd, J = 13.4, 6.1 Hz, 1H), 1.76 (dd, J = 13.4, 8.7 Hz, 1H), 1.39 (s, 3H), 1.26 (s, 3H); ^{13}C NMR (101 MHz, $CDCl_3$) δ 150.80, 148.48, 147.35, 145.14, 141.52, 127.67, 123.63, 115.23, 114.16, 101.17, 75.50, 70.88, 63.33, 55.81, 42.80, 28.83, 25.60; HRMS (ESI^+), calcd $C_{19}H_{21}LiNO_6$ (M + Li^+) = 366.1529, found = 366.1533.

Synthesis of 7-Methoxy-2,2-dimethyl-6-((4-nitrobenzyl)oxy)-2*H*-chromene (9). Compound **8** (200 mg, 0.56 mmol) was dissolved in acetone (10 mL) and then 4 N HCl (0.8 mL) was added. The reaction mixture was stirred overnight at room temperature. The reaction was basified with saturated $NaHCO_3$ solution and extracted with ethyl acetate. The combined organic layers were dried with Na_2SO_4, filtered, concentrated, and purified by flash column chromatography to afford the title compound **9** (176 mg, 93%) as a yellow solid. ^{1}H NMR (400 MHz, $CDCl_3$) δ 8.22 (d, J = 8.8 Hz, 2H), 7.61 (d, J = 8.9 Hz, 2H), 6.55 (s, 1H), 6.45 (s, 1H), 6.18 (d, J = 9.6 Hz, 1H), 5.48 (d, J = 9.7 Hz, 1H), 5.14 (s, 2H), 3.85 (s, 3H), 1.42 (s, 6H); ^{13}C NMR (101 MHz, $CDCl_3$) δ 150.77, 148.53, 147.44, 145.20, 141.42, 128.44, 127.66, 123.67, 121.64, 113.86, 113.26, 101.40, 76.19, 71.26, 55.94, 27.77; HRMS (ESI^+), calcd $C_{19}H_{19}LiNO_5$ ($M + Li^+$) = 348.1423, found = 348.1422.

2,2-Dimethyl-7-((4-nitrobenzyl)oxy)-2*H*-chromen-6-ol (12) was prepared using a similar procedure to compound 9. Yellow solid, yield 68% from compound **3**. ^{1}H NMR (400 MHz, $CDCl_3$) δ 8.28 (d, J = 8.7 Hz, 2H), 7.59 (d, J = 8.9 Hz, 2H), 6.64 (s, 1H), 6.40 (s, 1H), 6.25 (d, J = 9.7 Hz, 1H), 5.54 (d, J = 9.7 Hz, 1H), 5.20 (s, 2H), 1.41 (s, 6H); ^{13}C NMR (101 MHz, $CDCl_3$) δ 146.44, 145.15, 144.23, 143.52, 139.50, 129.31, 127.88, 123.98, 121.80, 115.18, 112.34, 101.55, 69.80, 27.59; HRMS (ESI^+), calcd $C_{18}H_{17}LiNO_5$ ($M + Li^+$) = 334.1267, found = 334.1262.

2,2-Diethyl-6,7-bis((4-nitrobenzyl)oxy)-2*H*-chromene (17a). Yellow solid, total yield 28%. ^{1}H NMR (400 MHz, $CDCl_3$) δ 8.25 (dd, J = 8.8, 4.5 Hz, 4H), 7.62 (dd, J = 8.9, 2.1 Hz, 4H), 6.59 (s, 1H), 6.44 (s, 1H), 6.30 (d, J = 10.0 Hz, 1H), 5.41 (d, J = 10.0 Hz, 1H), 5.22 (s, 2H), 5.17 (s, 2H), 1.77–1.68 (m, 2H), 1.65–1.59 (m, 2H), 0.93 (t, J = 7.4 Hz, 6H); ^{13}C NMR (101 MHz, $CDCl_3$) δ 149.49, 149.15, 147.59, 147.51, 145.04, 144.30, 141.61, 127.58, 127.48, 126.64,

123.81, 123.73, 122.90, 114.56, 114.35, 102.97, 82.02, 71.49, 69.77, 32.08, 7.99; HRMS (ESI^+), calcd $C_{27}H_{26}LiN_2O_7$ ($M + Li^+$) = 497.1900, found = 497.1909.

6,7-Bis((4-nitrobenzyl)oxy)spiro[chromene-2,1'-cyclohexane] (17b). Yellow solid, total yield 33%. ^1H NMR (400 MHz, $CDCl_3$) δ 8.25 (dd, J = 8.8, 6.1 Hz, 4H), 7.62 (dd, J = 8.9, 2.0 Hz, 4H), 6.62 (s, 1H), 6.51 (s, 1H), 6.22 (d, J = 9.7 Hz, 1H), 5.57 (d, J = 9.8 Hz, 1H), 5.23 (s, 2H), 5.18 (s, 2H), 1.95–1.86 (m, 2H), 1.77–1.68 (m, 2H), 1.60–1.33 (m, 6H); ^{13}C NMR (101 MHz, $CDCl_3$) δ 149.06, 148.41, 147.58, 147.50, 145.00, 144.29, 142.02, 128.94, 127.59, 127.49, 123.82, 123.73, 121.90, 115.53, 114.36, 103.68, 77.00, 71.39, 69.79, 35.74, 25.29, 21.35; HRMS (ESI^+), calcd $C_{28}H_{26}LiN_2O_7$ ($M + Li^+$) = 509.1900, found = 509.1900.

6,7-Bis((4-nitrobenzyl)oxy)spiro[chromene-2,1'-cyclopentane] (17c). Yellow solid, yield 30%. ^1H NMR (400 MHz, $CDCl_3$) δ 8.25 (dd, J = 8.8, 4.5 Hz, 4H), 7.64–7.60 (m, 4H), 6.62 (s, 1H), 6.44 (s, 1H), 6.24 (d, J = 9.7 Hz, 1H), 5.58 (d, J = 9.7 Hz, 1H), 5.21 (s, 2H), 5.18 (s, 2H), 2.17–2.10 (m, 2H), 1.91–1.84 (m, 2H), 1.74–1.67 (m, 2H), 1.62–1.56 (m, 2H); ^{13}C NMR (101 MHz, $CDCl_3$) δ 148.97, 148.53, 147.59, 147.51, 144.97, 144.27, 142.03, 128.28, 127.59, 127.47, 123.83, 123.74, 122.24, 115.41, 114.31, 103.65, 87.30, 71.40, 69.78, 39.16, 23.54; HRMS (ESI^+), calcd $C_{27}H_{24}LiN_2O_7$ ($M + Li^+$) = 495.1744, found = 495.1745.

6,7-Bis((4-nitrobenzyl)oxy)spiro[chromene-2,1'-cycloheptane] (17d). Yellow solid, total yield 24%. ^1H NMR (400 MHz, $CDCl_3$) δ 8.24 (dd, J = 8.8, 2.1 Hz, 4H), 7.62 (dd, J = 8.8, 3.6 Hz, 4H), 6.61 (s, 1H), 6.47 (s, 1H), 6.18 (d, J = 9.7 Hz, 1H), 5.59 (d, J = 9.7 Hz, 1H), 5.21 (s, 2H), 5.18 (s, 2H), 1.81–1.55 (m, 12H); ^{13}C NMR (101 MHz, $CDCl_3$) δ 149.03, 148.39, 147.94, 147.51, 145.00, 144.31, 141.97, 129.90, 127.59, 127.49, 123.81, 123.73, 120.52, 115.28, 114.27,

103.80, 81.05, 71.40, 69.79, 39.14, 29.56, 21.59; HRMS (ESI^+), calcd $C_{29}H_{28}LiN_2O_7$ ($M + Li^+$) = 523.2057, found = 523.2070.

General Procedure for the Preparation of Compounds 24a-e Exemplified by 6,7-Bis((4-nitrobenzyl)oxy)-2',3',5',6'-tetrahydrospiro[chromene-2,4'-pyran] (17e). A mixture of 1-(2-hydroxy-4,5-dimethoxyphenyl)ethan-1-one **1** (600 mg, 3.06 mmol), pyrrolidine (0.23 mL, 4.59mmol), tetrahydro-4*H*-pyran-4-one (0.32 mL, 4.59 mmol) and methanol (20 mL) was stirred at room temperature overnight. The reaction mixture was then concentrated in vacuo and the residue purified by flash chromatography to give 6,7-dimethoxy-2',3',5',6'-tetrahydrospiro[chromane-2,4'-pyran]-4-one **13e** (749 mg, 88%) as a white solid. ^1H NMR (400 MHz, $CDCl_3$) δ 7.26 (s, 1H), 6.47 (s, 1H), 3.93 (s, 3H), 3.87 (s, 3H), 3.86–3.80 (m, 2H), 3.79–3.74 (m, 2H), 2.68 (s, 2H), 2.02–1.97 (m, 2H), 1.80–1.73 (m, 2H); MS (ESI^+) m/z 279.1 $[M+H]^+$. To a solution of **13e** (600 mg, 2.16 mmol) in dichloromethane (20 mL) was slowly added boron tribromide (1M in dichloromethane, 6.47 mL, 6.47 mmol) at 0 ^oC under nitrogen. Then the reaction mixture was allowed to warm to room temperature and stirred overnight. The resultant mixture was poured into ice water, extracted with ethyl acetate for three times. The combined organic layers were dried with Na_2SO_4, filtered, concentrated, and purified by flash column chromatography to give 6,7-dihydroxy-2',3',5',6'-tetrahydrospiro[chromane-2,4'-pyran]-4-one **14e** (329 mg, 61%) as a white solid. ^1H NMR (400 MHz, CD_3OD) δ 7.16 (s, 1H), 6.37 (s, 1H), 3.75–3.67 (m, 2H), 3.59–3.48 (m, 2H), 2.77 (s, 2H), 2.41–2.31 (m, 2H), 2.04–1.96 (m, 2H); MS (ESI^+) m/z 251.1 $[M+H]^+$. To a mixture of **14e** (200 mg, 0.80 mmol) in dry THF (20 mL) was added portion-wise lithium aluminium hydride (91 mg, 1.67 mmol) at 0 ^oC. The reaction mixture was stirred at room temperature for 2 h then poured into water and extracted with ethyl acetate. The organic phase was concentrated to dryness to afford **15e**, which was carried out to

the next step without further purification. Compound **15e** was dissolved in acetone (10 mL) and then 4 N HCl (0.8 mL) was added. The reaction mixture was stirred at room temperature overnight. The reaction was basified with saturated $NaHCO_3$ solution and extracted with ethyl acetate. The combined organic layers were dried with Na_2SO_4, filtered, concentrated, and purified by flash column chromatography to afford 2',3',5',6'-tetrahydrospiro[chromene-2,4'-pyran]-6,7-diol **16e** (126 mg, 67% from compound **14e**) as a white solid. ^{1}H NMR (400 MHz, $CDCl_3$) δ 6.56 (s, 1H), 6.46 (s, 1H), 6.29 (d, J = 9.7 Hz, 1H), 6.21 (s, 1H), 5.50 (s, 1H), 5.49 (d, J = 9.7 Hz, 1H), 3.98–3.91 (m, 2H), 3.81–3.76 (m, 2H), 2.00–1.95 (m, 2H), 1.81–1.75 (m, 2H); MS (ESI^+) m/z 235.1 $[M+H]^+$. A mixture of **16e** (100 mg, 0.43 mmol) and potassium carbonate (354 mg, 2.56 mmol) in acetone (20 mL) was treated with 4-nitrobenzyl bromide (203 mg, 0.94 mmol) and stirred at 60 ^{o}C under nitrogen overnight. The reaction mixture was filtered, concentrated, and purified by flash column chromatography to give the title compound **17e** (183 mg, 85%) as a yellow solid. ^{1}H NMR (400 MHz, $CDCl_3$) δ 8.26 (t, J = 8.6 Hz, 4H), 7.63 (dd, J = 8.8, 6.4 Hz, 4H), 6.64 (s, 1H), 6.55 (s, 1H), 6.29 (d, J = 9.7 Hz, 1H), 5.54 (d, J = 9.7 Hz, 1H), 5.24 (s, 2H), 5.19 (s, 2H), 3.89 (td, J = 11.2, 2.6 Hz, 2H), 3.76 (dt, J = 11.6, 4.2 Hz, 2H), 1.95 (d, J = 12.7 Hz, 2H), 1.81–1.74 (m, 2H); ^{13}C NMR (101 MHz, $CDCl_3$) δ 149.31, 147.85, 147.66, 147.57, 144.80, 144.07, 142.37, 127.57, 127.50, 123.86, 123.77, 122.76, 115.13, 114.45, 103.71, 74.20, 71.35, 69.84, 63.24, 35.69; HRMS (ESI^+), calcd $C_{27}H_{24}LiN_2O_8$ ($M + Li^+$) = 511.1693, found = 511.1697.

Synthesis of 2,2-Dimethyl-2*H*-chromene-6,7-diyl bis(4-nitrobenzoate) (18). To a mixture of 2,2-dimethyl-2*H*-chromene-6,7-diol **16f** (100 mg, 0.52 mmol) and triethylamine (0.18 mL, 1.30 mmol) in dichloromethane (20 mL) was added 4-nitrobenzoyl chloride (241 mg, 1.30 mmol), and the reaction was stirred overnight. The reaction mixture was concentrated and

purified by flash column chromatography to give the title compound **18** (189 mg, 74%) as a yellow solid. ^{1}H NMR (400 MHz, $CDCl_3$) δ 8.27–8.22 (m, 8H), 7.02 (s, 1H), 6.82 (s, 1H), 6.32 (d, J = 9.9 Hz, 1H), 5.71 (d, J = 9.9 Hz, 1H), 1.49 (s, 6H); ^{13}C NMR (101 MHz, $CDCl_3$) δ 162.61, 162.12, 151.54, 150.98, 150.95, 141.44, 135.04, 134.04, 133.91, 131.76, 131.17, 131.11, 123.78, 123.77, 120.87, 120.13, 120.08, 111.25, 77.07, 28.13; HRMS (ESI^+), calcd $C_{25}H_{18}LiN_2O_9$ ($M + Li^+$) = 497.1172, found = 497.1171.

Reagents. TLR ligands Pam_3CSK_4, Pam_2CSK_4, poly I:C, lipopolysaccharide, flagellin, R848, ODN2006 were purchased from InvivoGen (San Diego, CA, USA). Phorbol 12-myristate 13-acetate (PMA) and WST-1 proliferation reagent were purchased from Sigma-Aldrich (St. Louis, MO, USA). RNeasy Mini kit and RT^2 First Strand kit were purchased from QIAGEN (Valencia, CA, USA). SsoAdvanced Universal SYBR Green Supermix for qPCR was purchased from BioRad (Hercules, CA, USA). The primers for TNF-α (Accession #: NM_000594), IL-6 (Accession #: NM_000600), IL-8 (Accession #: NM_000584), and GAPDH (Accession #: NM_002046) were purchased from QIAGEN (Valencia, CA, USA). ELISA kit and FITC Annexin V Apoptosis Detection kit were purchased from BD Biosciences (San Jose, CA, USA). Cell Cycle Phase Determination kit was purchased from Cayman Chemical (Ann Arbor, MI, USA). All the synthesized small molecules were dissolved in dimethyl sulfoxide at 10 mM as a stock solution.

Cell culture. HEK293 cells stably transfected with human TLR2, TLR3, TLR4, TLR5, TLR7, TLR8, or TLR9 and a SEAP reporter gene were obtained from InvivoGen. SEAP expression is maintained by culturing the cells in Dulbecco's modified Eagle's medium (DMEM) supplemented with 10% fetal bovine serum (FBS), 1% PenStrep (100 U/mL Penicillin and 100 µg/mL Streptomycin) containing selective antibiotics such as Zeocin and/or Blasticidin

(InvivoGen) according to the manufacturer's instructions. THP-1 cells were cultured in RPMI 1640 medium supplemented with 10% FBS and 1% PenStrep. Human cervical adenocarcinoma HeLa cells were cultured in DMEM supplemented with 10% FBS and 1% PenStrep. All the cells were maintained in a humidified incubator containing 5% CO_2 at 37 ^oC.

High-throughput screening. The HTS was carried out at the HTS core facility of the University of Colorado at Boulder. Briefly, hTLR3 HEK293 cells were seeded at 20,000 cells/well in duplicate in 384-well plates. Poly I:C was used as a positive control at 5 μg/mL. Various instruments such as CyBi-Well, 96- and 384-channel simultaneous pipettor, precision microplate pipetting system, EL406 combination washer dispenser, PlateLoc Thermal microplate sealer and EnVision multilabel plate reader were used to carry out the screening. The library compounds were dissolved in DMSO and used at 30 μM in the screening.

NF-κB activation by QUANTI-Blue SEAP assay. HEK293 cells seeded at a density of 5×10^4 cells/well in 96-well plates for 24 h at 37 ^oC before treatment. The positive control ligands for different TLRs are Pam_3CSK_4 for TLR1/2, poly I:C for TLR3, lipopolysaccharide for TLR4, FLA-BS for TLR5, R848 for TLR7 and TLR8, and ODN2006 for TLR9. After treatment for 24 h, a sample buffer (20 μL) from each well of the cell culture supernatants was collected and transferred to a transparent 96-well plate. Each well was treated with 180 μL of QUANTI-Blue (InvivoGen) buffer and incubated at 37 ^oC for 1 h. Optical density was measured using a plate reader (Beckman Coulter, DTX 880) at an absorbance of 620 nm.

WST-1 assay for cell growth inhibition. Cells were seeded at a density of 5×10^3 cells/well in 100 μL of culture medium in 96-well plates and incubated for 24 h. A series of concentrations of indicated compounds were added to the wells and incubated for additional 24, 48, or 72 h.

WST-1 proliferation reagent (10 μL/well) was added and incubated at 37 °C until a color change was observed (30 min to 2 h). Data were quantified on a Beckman-Coulter DTX 880 Multimode Detector using absorbance at 450 nm. Growth inhibition (%) was determined using the following formula: Growth inhibition (%) = (1 – [Compounds (OD_{450}) – Background (OD_{450})]/[Control (OD_{450}) – Background (OD_{450})]) × 100.

qRT-PCR. THP-1 cells were seeded at a density of 1.5×10^6 cells/well in RPMI 1640 growth medium in 6□well plates. Cells were differentiated with PMA (20 nM) for 2 days then grown in fresh RPMI 1640 medium for additional 24 h. Nonadherent cells and medium were removed and replaced with fresh RPMI 1640 medium. The cells were treated with the indicated concentrations of compounds then incubated for 12 h. Cells were collected after washing with phosphate buffered saline, and frozen at -70 °C until ready for assay. Total RNA was extracted with an RNeasy Mini kit (QIAGEN) according to the manufacturer's instruction. Reverse transcription was performed on a BioRad T100 thermal cycler with a Qiagen RT^2 First Strand kit. qPCR was performed on a Bio-Rad CFX96 Real-Time PCR system using the SYBR Green method. The data were analyzed by $\Delta\Delta C_t$ method.

Cytokine-specific ELISA. THP-1 cells were seeded at a density of 1.5×10^6 cells/well in RPMI 1640 growth medium in 6□well plates. Cells were differentiated with PMA (20 nM) for 2 days then grown in fresh RPMI 1640 medium for additional 24 h. Nonadherent cells and medium were removed and replaced with fresh RPMI 1640 medium. The cells were treated with the indicated concentrations of compounds then incubated for 24 h. The cell culture supernatants were collected and frozen at -70 °C until ready for cytokine measurement with a ELISA kit (BD Biosciences) per manufacturer's specifications.

Apoptosis assay. HeLa cells were seeded at a density of 3×10^5 cells/well in 6-well plates and allowed to attach for 24 h. After treatment of indicated concentrations of **17e** or poly I:C (5 μg/ml) for another 24 h, cells were harvested with 0.25% trypsin without EDTA and rinsed twice with PBS, then stained using a Annexin V-FITC apoptosis detection kit (BD Biosciences) per manufacturer's instructions. Cells were analyzed with a BD Accuri C6 flow cytometer (BD Biosciences).

Cell cycle analysis. HeLa cells were seeded at a density of 3×10^5 cells/well in 6-well plates and allowed to attach overnight. The culture medium was changed to serum-free to facilitate cycle synchronization prior to treatment with indicated concentrations of **17e** or poly I:C (5 μg/mL). After 24 h, cells were harvested with 0.25% trypsin without EDTA, washed twice with assay buffer (Cayman Chemical) and pelleted. Cell pellets were fixed and stained using a Cell Cycle Phase Determination kit (Cayman Chemical) per manufacturer's instructions. Cells were analyzed with a BD Accuri C6 flow cytometer (BD Biosciences).

Statistical Analysis. All data from cell culture experiments were performed on the basis of three individual cell preparations unless otherwise noted. Data are expressed as mean ± standard deviation (SD). Statistical significances were determined with use of the unpaired Student's t test. Values of $p < 0.05$ were considered as statistically significant.

AUTHOR INFORMATION

Corresponding Author

*Phone: 303-492 6786. E-mail: hubert.yin@colorado.edu.

Supporting Information. Molecular Formula Strings; Figure S1, ^{1}H and ^{13}C NMR spectra for products **4a-h**, **5a-h**, **6a-h**, **9**, **10**, **12**, **17a-e**, and **18**. This material is available free of charge via the Internet at http://pubs.acs.org.

Acknowledgments. We are grateful to Prof. Xiang Wang, Director of the High-Throughput Screening Core Facility at the University of Colorado at Boulder, and his colleague Wei Wang for assistance with plating compounds. We thank Theresa Nahreini, manager of the Cell Culture Facility at the University of Colorado Boulder, for providing the HuMEC and cancer cell lines. We thank Dr. Adam Csakai for helpful discussions on chemical synthesis.

Author Contributions. V.D. carried out the HTS. L.Z. designed the project, conducted the chemical synthesis, SAR studies, all biological tests, and analyzed the data. L.Z, V.D., and H.Y. drafted the manuscript. All authors read and approved the final manuscript.

Funding Sources. This study was supported by grants from NIH (R01GM101279).

Competing interests. The authors declare no competing financial interest.

Abbreviations. TLR, Toll-like receptor; PRRs, pattern recognition receptors; NF-κB, nuclear factor-κB; TNF-α, tumor necrosis factor α; IL, interleukin; poly I:C, polyribosinic:polyribocytidic acid; BCG, Bacillus Calmette-Guérin; HTS, high-throughput screening; SAR, structure-activity relationship; SEAP, secreted embryonic alkaline phosphatase; RMS, root mean square; DMSO, dimethyl sulfoxide; rt, room temperature; ELISA, enzyme-linked immunosorbent assay; HuMEC, human mammary epithelial cells; PI, propidium iodide; FITC, fluorescein isothiocyanate; PS, phosphatidylserine.

References

(1) Akira, S.; Uematsu, S.; Takeuchi, O. Pathogen recognition and innate immunity. *Cell* **2006**, *124*, 783-801.

(2) Bryant, C. E.; Gay, N. J.; Heymans, S.; Sacre, S.; Schaefer, L.; Midwood, K. S. Advances in Toll-like receptor biology: modes of activation by diverse stimuli. *Crit. Rev. Biochem. Mol. Biol.* **2015**, *50*, 359-379.

(3) Sato, Y.; Goto, Y.; Narita, N.; Hoon, D. S. Cancer cells expressing Toll-like receptors and the tumor microenvironment. *Cancer Microenviron.* **2009**, *2*, 205-214.

(4) Rakoff-Nahoum, S.; Medzhitov, R. Toll-like receptors and cancer. *Nat. Rev. Cancer* **2009**, *9*, 57-63.

(5) Iribarren, K.; Bloy, N.; Buqué, A.; Cremer, I.; Eggermont, A.; Fridman, W. H.; Fucikova, J.; Galon, J.; Špíšek, R.; Zitvogel, L.; Kroemer, G.; Galluzzi, L. Trial watch: immunostimulation with Toll-like receptor agonists in cancer therapy. *OncoImmunology* **2016**, *5*, e1088631.

(6) Vacchelli, E.; Galluzzi, L.; Eggermont, A.; Fridman, W. H.; Galon, J.; Sautes-Fridman, C.; Tartour, E.; Zitvogel, L.; Kroemer, G. Trial watch: FDA-approved Toll-like receptor agonists for cancer therapy. *Oncoimmunology* **2012**, *1*, 894-907.

(7) Cheever, M. A. Twelve immunotherapy drugs that could cure cancers. *Immunol. Rev.* **2008**, *222*, 357-368.

(8) Hajishengallis, G.; Lambris, J. D. Crosstalk pathways between Toll-like receptors and the complement system. *Trends Immunol.* **2010**, *31*, 154-163.

(9) Tan, R. S.; Ho, B.; Leung, B. P.; Ding, J. L. TLR cross-talk confers specificity to innate immunity. *Int. Rev. Immunol.* **2014**, *33*, 443-453.

(10) Hajishengallis, G.; Lambris, J. D. More than complementing tolls: complement-Toll-like receptor synergy and crosstalk in innate immunity and inflammation. *Immunol. Rev.* **2016**, *274*, 233-244.

(11) Napolitani, G.; Rinaldi, A.; Bertoni, F.; Sallusto, F.; Lanzavecchia, A. Selected Toll-like receptor agonist combinations synergistically trigger a T helper type 1-polarizing program in dendritic cells. *Nat. Immunol.* **2005**, *6*, 769-776.

(12) Trinchieri, G.; Sher, A. Cooperation of Toll-like receptor signals in innate immune defence. *Nat. Rev. Immunol.* **2007**, *7*, 179-190.

(13) Liu, Q.; Ding, J. L. The molecular mechanisms of TLR-signaling cooperation in cytokine regulation. *Immunol. Cell Biol.* **2016**, *94*, 538-542.

(14) Peters, B. M.; Jabra-Rizk, M. A.; O'May, G. A.; Costerton, J. W.; Shirtliff, M. E. Polymicrobial interactions: impact on pathogenesis and human disease. *Clin. Microbiol. Rev.* **2012**, *25*, 193-213.

(15) Murray, J. L.; Connell, J. L.; Stacy, A.; Turner, K. H.; Whiteley, M. Mechanisms of synergy in polymicrobial infections. *J. Microbiol.* **2014**, *52*, 188-199.

(16) Thaiss, C. A.; Levy, M.; Itav, S.; Elinav, E. Integration of innate immune signaling. *Trends Immunol.* **2016**, *37*, 84-101.

(17) Iwasaki, A.; Medzhitov, R. Toll-like receptor control of the adaptive immune responses. *Nat. Immunol.* **2004**, *5*, 987-995.

(18) Kadowaki, N.; Ho, S.; Antonenko, S.; de Waal Malefyt, R.; Kastelein, R. A.; Bazan, F.; Liu, Y.-J. Subsets of human dendritic cell precursors express different Toll-like receptors and respond to different microbial antigens. *J. Exp. Med.* **2001**, *194*, 863-870.

(19) Hussein, W. M.; Liu, T. Y.; Skwarczynski, M.; Toth, I. Toll-like receptor agonists: a patent review (2011-2013). *Expert. Opin. Ther. Pat.* **2014**, *24*, 453-470.

(20) Hennessy, E. J.; Parker, A. E.; O'Neill, L. A. Targeting Toll-like receptors: emerging therapeutics? *Nat. Rev. Drug Discovery* **2010**, *9*, 293-307.

(21) Kaczanowska, S.; Joseph, A. M.; Davila, E. TLR agonists: our best frenemy in cancer immunotherapy. *J. Leukocyte. Biol.* **2013**, *93*, 847-863.

(22) Duthie, M. S.; Windish, H. P.; Fox, C. B.; Reed, S. G. Use of defined TLR ligands as adjuvants within human vaccines. *Immunol. Rev.* **2011**, *239*, 178-196.

(23) Zhu, Q.; Egelston, C.; Vivekanandhan, A.; Uematsu, S.; Akira, S.; Klinman, D. M.; Belyakov, I. M.; Berzofsky, J. A. Toll-like receptor ligands synergize through distinct dendritic cell pathways to induce T cell responses: implications for vaccines. *Proc. Natl. Acad. Sci. U.S.A.* **2008**, *105*, 16260-16265.

(24) Warger, T.; Osterloh, P.; Rechtsteiner, G.; Fassbender, M.; Heib, V.; Schmid, B.; Schmitt, E.; Schild, H.; Radsak, M. P. Synergistic activation of dendritic cells by combined Toll-like receptor ligation induces superior CTL responses in vivo. *Blood* **2006**, *108*, 544-550.

(25) Hansen, B. S.; Hussain, R. Z.; Lovett-Racke, A. E.; Thomas, J. A.; Racke, M. K. Multiple Toll-like receptor agonists act as potent adjuvants in the induction of autoimmunity. *J. Neuroimmunol.* **2006**, *172*, 94-103.

(26) Raman, V. S.; Bhatia, A.; Picone, A.; Whittle, J.; Bailor, H. R.; O'Donnell, J.; Pattabhi, S.; Guderian, J. A.; Mohamath, R.; Duthie, M. S.; Reed, S. G. Applying TLR synergy in immunotherapy: implications in cutaneous leishmaniasis. *J. Immunol.* **2010**, *185*, 1701-1710.

(27) Goff, P. H.; Hayashi, T.; Martínez-Gil, L.; Corr, M.; Crain, B.; Yao, S.; Cottam, H. B.; Chan, M.; Ramos, I.; Eggink, D.; Heshmati, M.; Krammer, F.; Messer, K.; Pu, M.; Fernandez-

Sesma, A.; Palese, P.; Carson, D. A. Synthetic Toll-like receptor 4 (TLR4) and TLR7 ligands as influenza virus vaccine adjuvants induce rapid, sustained, and broadly protective responses. *J. Virol.* **2015**, *89*, 3221-3235.

(28) Pulendran, B. Learning immunology from the yellow fever vaccine: innate immunity to systems vaccinology. *Nat. Rev. Immunol.* **2009**, *9*, 741-747.

(29) Querec, T.; Bennouna, S.; Alkan, S.; Laouar, Y.; Gorden, K.; Flavell, R.; Akira, S.; Ahmed, R.; Pulendran, B. Yellow fever vaccine YF-17D activates multiple dendritic cell subsets via TLR2, 7, 8, and 9 to stimulate polyvalent immunity. *J. Exp. Med.* **2006**, *203*, 413-424.

(30) Zhu, Q.; Egelston, C.; Gagnon, S.; Sui, Y.; Belyakov, I. M.; Klinman, D. M.; Berzofsky, J. A. Using 3 TLR ligands as a combination adjuvant induces qualitative changes in T cell responses needed for antiviral protection in mice. *J. Clin. Invest.* **2010**, *120*, 607-616.

(31) Redelman-Sidi, G.; Glickman, M. S.; Bochner, B. H. The mechanism of action of BCG therapy for bladder cancer -- a current perspective. *Nat. Rev. Urol.* **2014**, *11*, 153-162.

(32) Conforti, R.; Ma, Y.; Morel, Y.; Paturel, C.; Terme, M.; Viaud, S.; Ryffel, B.; Ferrantini, M.; Uppaluri, R.; Schreiber, R.; Combadière, C.; Chaput, N.; André, F.; Kroemer, G.; Zitvogel, L. Opposing effects of Toll-like receptor (TLR3) signaling in tumors can be therapeutically uncoupled to optimize the anticancer efficacy of TLR3 ligands. *Cancer Res.* **2010**, *70*, 490-500.

(33) Whitmore, M. M.; DeVeer, M. J.; Edling, A.; Oates, R. K.; Simons, B.; Lindner, D.; Williams, B. R. G. Synergistic activation of innate immunity by double-stranded RNA and CpG DNA promotes enhanced antitumor activity. *Cancer Res.* **2004**, *64*, 5850-5860.

(34) Zhao, B. G.; Vasilakos, J. P.; Tross, D.; Smirnov, D.; Klinman, D. M. Combination therapy targeting Toll like receptors 7, 8 and 9 eliminates large established tumors. *J. Immunother. Cancer* **2014**, *2*, 12.

(35) Mancini, R. J.; Tom, J. K.; Esser-Kahn, A. P. Covalently coupled immunostimulant heterodimers. *Angew. Chem. Int. Ed.* **2014**, *53*, 189-192.

(36) Pavot, V.; Rochereau, N.; Rességuier, J.; Gutjahr, A.; Genin, C.; Tiraby, G.; Perouzel, E.; Lioux, T.; Vernejoul, F.; Verrier, B.; Paul, S. Cutting edge: new chimeric NOD2/TLR2 adjuvant drastically increases vaccine immunogenicity. *J. Immunol.* **2014**, *193*, 5781-5785.

(37) Tom, J. K.; Dotsey, E. Y.; Wong, H. Y.; Stutts, L.; Moore, T.; Davies, D. H.; Felgner, P. L.; Esser-Kahn, A. P. Modulation of innate immune responses via covalently linked TLR agonists. *ACS Cent. Sci.* **2015**, *1*, 439-448.

(38) Shukla, N. M.; Mutz, C. A.; Malladi, S. S.; Warshakoon, H. J.; Balakrishna, R.; David, S. A. Toll-like receptor (TLR)-7 and -8 modulatory activities of dimeric imidazoquinolines. *J. Med. Chem.* **2012**, *55*, 1106-1116.

(39) Shukla, N. M.; Salunke, D. B.; Balakrishna, R.; Mutz, C. A.; Malladi, S. S.; David, S. A. Potent adjuvanticity of a pure TLR7-agonistic imidazoquinoline dendrimer. *PLoS One* **2012**, *7*, e43612.

(40) Engel, A. L.; Holt, G. E.; Lu, H. The pharmacokinetics of Toll-like receptor agonists and the impact on the immune system. *Expert Rev. Clin. Pharmacol.* **2011**, *4*, 275-289.

(41) Mancini, R. J.; Stutts, L.; Ryu, K. A.; Tom, J. K.; Esser-Kahn, A. P. Directing the immune system with chemical compounds. *ACS Chem. Biol.* **2014**, *9*, 1075-1085.

(42) Salyer, A. C. D.; Caruso, G.; Khetani, K. K.; Fox, L. M.; Malladi, S. S.; David, S. A. Identification of adjuvantic activity of Amphotericin B in a novel, multiplexed, poly-TLR/NLR high-throughput screen. *PLOS ONE* **2016**, *11*, e0149848.

(43) Kawai, T.; Akira, S. Innate immune recognition of viral infection. *Nat. Immunol.* **2006**, *7*, 131-137.

(44) Zhang, J.-H.; Chung, T. D. Y.; Oldenburg, K. R. A simple statistical parameter for use in evaluation and validation of high throughput screening assays. *J. Biomol. Screen.* **1999**, *4*, 67-73.

(45) Das, N.; Dewan, V.; Grace, Peter M.; Gunn, Robin J.; Tamura, R.; Tzarum, N.; Watkins, Linda R.; Wilson, Ian A.; Yin, H. HMGB1 activates proinflammatory signaling via TLR5 leading to allodynia. *Cell Rep.* **2016**, *17*, 1128-1140.

(46) Timár, T.; Jászberényi, J. C. A novel synthesis of precocenes. Efficient synthesis and regioselective O-alkylation of dihydroxy-2,2-dimethyl-4-chromanones. *J Heterocycl Chem.* **1988**, *25*, 871-877.

(47) Yin, H. Novel immunomodulators that target toll-like receptors. In: The 252nd ACS National Meeting in Philadelphia; Aug 21-25, **2016**; Philadelphia, PA. MEDI 246.

(48) Zhang, C.; Bai, N.; Chang, A.; Zhang, Z.; Yin, J.; Shen, W.; Tian, Y.; Xiang, R.; Liu, C. ATF4 is directly recruited by TLR4 signaling and positively regulates TLR4-trigged cytokine production in human monocytes. *Cell. Mol. Immunol.* **2013**, *10*, 84-94.

(49) Paone, A.; Galli, R.; Gabellini, C.; Lukashev, D.; Starace, D.; Gorlach, A.; De Cesaris, P.; Ziparo, E.; Del Bufalo, D.; Sitkovsky, M. V.; Filippini, A.; Riccioli, A. Toll-like receptor 3 regulates angiogenesis and apoptosis in prostate cancer cell lines through hypoxia-inducible factor 1 alpha. *Neoplasia* **2010**, *12*, 539-549.

(50) Dogusan, Z.; García, M.; Flamez, D.; Alexopoulou, L.; Goldman, M.; Gysemans, C.; Mathieu, C.; Libert, C.; Eizirik, D. L.; Rasschaert, J. Double-stranded RNA induces pancreatic β-cell apoptosis by activation of the Toll-like receptor 3 and interferon regulatory factor 3 pathways. *Diabetes* **2008**, *57*, 1236-1245.

(51) Salaun, B.; Coste, I.; Rissoan, M.-C.; Lebecque, S. J.; Renno, T. TLR3 can directly trigger apoptosis in human cancer cells. *J. Immunol.* **2006**, *176*, 4894-4901.

(52) Fadok, V. A.; Voelker, D. R.; Campbell, P. A.; Cohen, J. J.; Bratton, D. L.; Henson, P. M. Exposure of phosphatidylserine on the surface of apoptotic lymphocytes triggers specific recognition and removal by macrophages. *J. Immunol.* **1992**, *148*, 2207-2216.

(53) Martin, S. J.; Reutelingsperger, C. P.; McGahon, A. J.; Rader, J. A.; van Schie, R. C.; LaFace, D. M.; Green, D. R. Early redistribution of plasma membrane phosphatidylserine is a general feature of apoptosis regardless of the initiating stimulus: inhibition by overexpression of Bcl-2 and Abl. *J. Exp. Med.* **1995**, *182*, 1545-1556.

(54) Giordano, S.; Petrelli, A. From single- to multi-target drugs in cancer therapy: when aspecificity becomes an advantage. *Curr. Med. Chem.* **2008**, *15*, 422-432.

(55) Zimmermann, G. R.; Lehár, J.; Keith, C. T. Multi-target therapeutics: when the whole is greater than the sum of the parts. *Drug Discovery Today* **2007**, *12*, 34-42.

(56) Medina-Franco, J. L.; Giulianotti, M. A.; Welmaker, G. S.; Houghten, R. A. Shifting from the single to the multitarget paradigm in drug discovery. *Drug Discovery Today* **2013**, *18*, 495-501.

(57) Koeberle, A.; Werz, O. Multi-target approach for natural products in inflammation. *Drug Discovery Today* **2014**, *19*, 1871-1882.

(58) Huang, S.; Kauffman, S. How to escape the cancer attractor: rationale and limitations of multi-target drugs. *Semin. Cancer Biol.* **2013**, *23*, 270-278.

(59) O'Neill, L. A. J.; Bryant, C. E.; Doyle, S. L. Therapeutic targeting of toll-like receptors for infectious and inflammatory diseases and cancer. *Pharmacol. Rev.* **2009**, *61*, 177-197.

(60) Botos, I.; Segal, David M.; Davies, David R. The structural biology of Toll-like receptors. *Structure* **2011**, *19*, 447-459.

(61) Miyake, K. Nucleic acid-sensing Toll-like receptors: beyond ligand search. *Adv. Drug Delivery Rev.* **2008**, *60*, 782-785.

(62) Diebold, S. S. Recognition of viral single-stranded rna by Toll-like receptors. *Adv. Drug Delivery Rev.* **2008**, *60*, 813-823.

(63) Lee, J.; Chuang, T. H.; Redecke, V.; She, L.; Pitha, P. M.; Carson, D. A.; Raz, E.; Cottam, H. B. Molecular basis for the immunostimulatory activity of guanine nucleoside analogs: activation of Toll-like receptor 7. *Proc. Natl. Acad. Sci. U.S.A.* **2003**, *100*, 6646-6651.

(64) Gorden, K. B.; Gorski, K. S.; Gibson, S. J.; Kedl, R. M.; Kieper, W. C.; Qiu, X.; Tomai, M. A.; Alkan, S. S.; Vasilakos, J. P. Synthetic TLR agonists reveal functional differences between human TLR7 and TLR8. *J. Immunol.* **2005**, *174*, 1259-1268.

(65) Lan, T.; Dai, M.; Wang, D.; Zhu, F.-G.; Kandimalla, E. R.; Agrawal, S. Toll-like receptor 7 selective synthetic oligoribonucleotide agonists: synthesis and structure-activity relationship studies. *J. Med. Chem.* **2009,** *52*, 6871-6879.

(66) Schiaffo, C. E.; Shi, C.; Xiong, Z.; Olin, M.; Ohlfest, J. R.; Aldrich, C. C.; Ferguson, D. M. Structure-activity relationship analysis of imidazoquinolines with Toll-like receptors 7 and 8 selectivity and enhanced cytokine induction. *J. Med. Chem.* **2014**, *57*, 339-347.

(67) Maródi, L. Innate cellular immune responses in newborns. *Clin. Immunol.* **2006**, *118*, 137-144.

(68) Van Duin, D.; Shaw, A. C. Toll-like receptors in older adults. *J. Am. Geriatr. Soc.* **2007**, *55*, 1438-1444.

(69) Hartwell, L.; Kastan, M. Cell cycle control and cancer. *Science* **1994**, *266*, 1821-1828.

Scheme 1. Synthetic routes of 2,2-dimethyl-2*H*-chromenes **6a-h**, **9**, and **12**.[a]

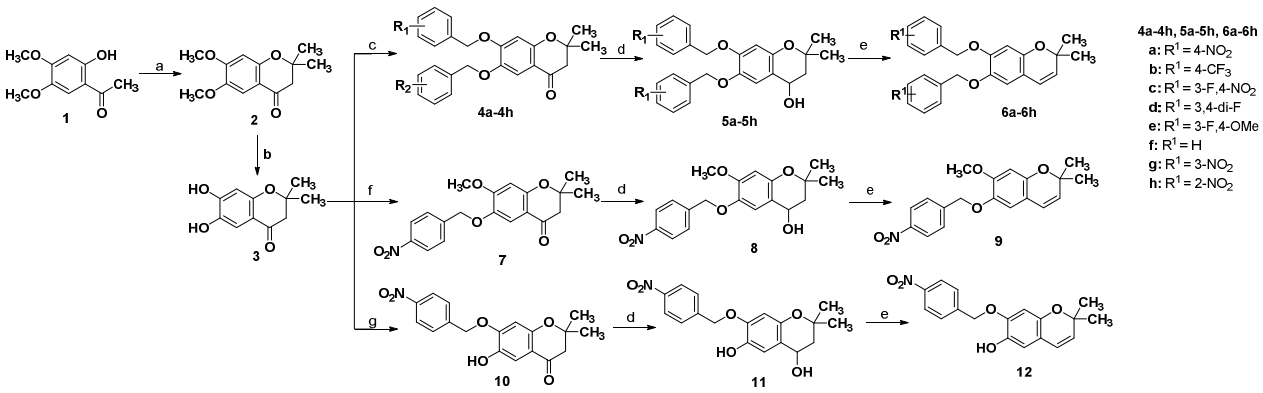

[a]Reagents and conditions: (a) acetone, pyrrolidine, CH_3OH, reflux; (b) BBr_3, CH_2Cl_2, 0 ^oC then rt; (c) substituted benzyl bromides, K_2CO_3, acetone, reflux; (d) $NaBH_4$, CH_3OH, reflux; (e) 4 N HCl, acetone, rt; (f) i) CH_3I, K_2CO_3, DMF, 80 ^oC, ii) 4-nitrobenzyl bromide, K_2CO_3, DMF, rt; (g) 4-nitrobenzyl bromide (1.0 equiv), K_2CO_3, acetone, reflux.

Scheme 2. Synthetic routes of coumarins **17a-e** and **18**.[a]

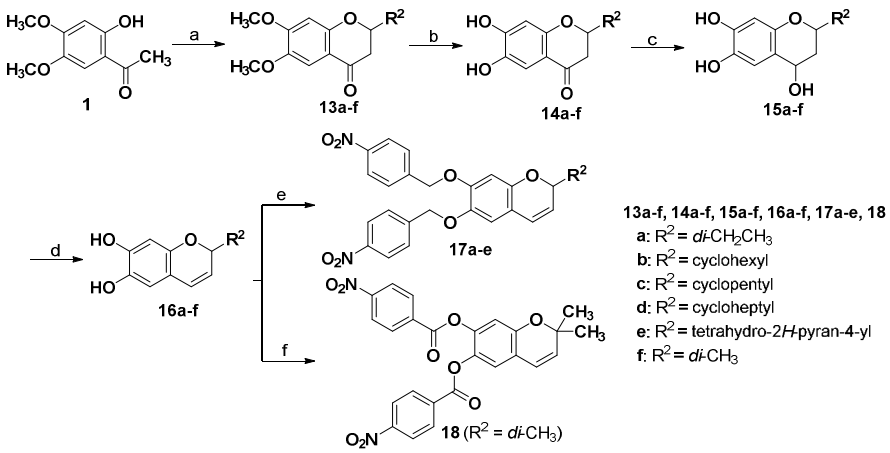

[a]Reagents and conditions: (a) substituted ketones, pyrrolidine, CH_3OH, reflux; (b) BBr_3, CH_2Cl_2, 0 ^oC then rt; (c) $LiAlH_4$, THF, 0 ^oC then rt; (d) 4 N HCl, acetone, rt; (e) 4-nitrobenzyl bromide, K_2CO_3, acetone, reflux; (f) 4-nitrobenzoyl chloride, Et_3N, CH_2Cl_2, rt.

Table 1. SAR studies of compounds **6a**, **9**, **12**, and **18** in hTLR3 HEK293 cells.

Structure	Compd	NF-κB activation	
		Activation fold at 25 μM [a]	EC_{50} (μM)[a]
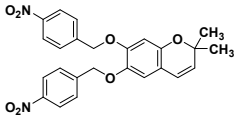	**6a**	5.34 ± 0.43	22.33 ± 5.34
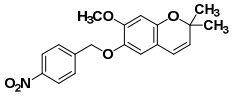	**9**	1.19 ± 0.08	ND[b]
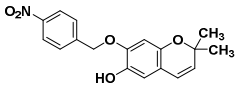	**12**	1.17 ± 0.09	ND[b]
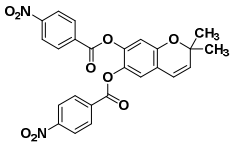	**18**	1.65 ± 0.15	ND[b]

[a]Data were mean ± SD. [b]ND: Not determined.

Table 2. SAR studies of compounds **4a-e**, **5a-e**, and **6a-h** in hTLR3 HEK293 cells.

Structure		Compd	NF-κB activation	
Generic Structure	R_1		Activation fold at 25 μM [a]	EC_{50} (μM)[a]
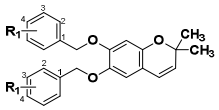 chromenes	4-NO_2	**6a**	5.34 ± 0.43	22.33 ± 5.34
	4-CF_3	**6b**	0.99 ± 0.02	ND[b]
	3-F,4-NO_2	**6c**	1.24 ± 0.09	ND[b]
	3,4-*di*-F	**6d**	0.99 ± 0.09	ND[b]
	3-F,4-OMe	**6e**	1.06 ± 0.07	ND[b]
	H	**6f**	1.09 ± 0.03	ND[b]
	3-NO_2	**6g**	1.10 ± 0.06	ND[b]
	2-NO_2	**6h**	1.08 ± 0.03	ND[b]
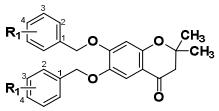 chromones	4-NO_2	**4a**	1.76 ± 0.07	ND[b]
	4-CF_3	**4b**	1.19 ± 0.03	ND[b]
	3-F,4-NO_2	**4c**	1.22 ± 0.07	ND[b]
	3,4-*di*-F	**4d**	1.22 ± 0.14	ND[b]
	3-F,4-OMe	**4e**	1.08 ± 0.04	ND[b]
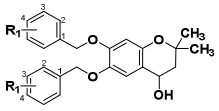 chromanols	4-NO_2	**5a**	2.50 ± 0.50	42.50 ± 4.37
	4-CF_3	**5b**	2.36 ± 0.03	ND[b]
	3-F,4-NO_2	**5c**	2.34 ± 0.78	ND[b]
	3,4-*di*-F	**5d**	0.95 ± 0.04	ND[b]
	3-F,4-OMe	**5e**	1.34 ± 0.11	ND[b]

[a]Data were mean ± SD. [b]ND: Not determined.

Table 3. SAR studies of compounds **17a-e** in hTLR3 HEK293 cells.

Structure	Compd	NF-κB activation	
		Activation fold at 25 μM [a]	EC_{50} (μM)[a]
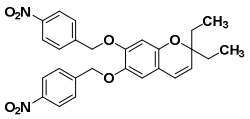	**17a**	1.16 ± 0.03	ND[b]
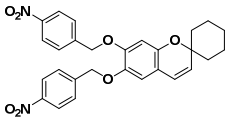	**17b**	1.00 ± 0.05	ND[b]
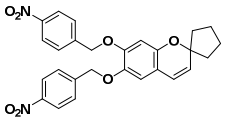	**17c**	1.22 ± 0.09	ND[b]
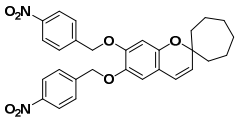	**17d**	1.07 ± 0.02	ND[b]
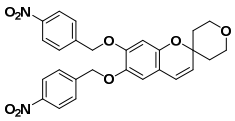	**17e** **(CU-CPT17e)**	13.93 ± 0.93	**4.80 ± 0.73**

[a]Data were mean ± SD. [b]ND: Not determined.

Table 4. NF-κB activation of **17e** by the SEAP assay in HEK293 cells overexpressing individual hTLRs.

hTLR	**NF-κB activation**
HEK293 cells	**EC_{50} (μM)**[a]
TLR2	> 100
TLR3	**4.80 ± 0.73**
TLR4	> 100
TLR5	> 100
TLR7	> 100
TLR8	**13.45 ± 0.58**
TLR9	**5.66 ± 0.17**

[a]Data were mean ± SD.

Table 5. Cytotoxicity of compound **17e** in HeLa and HuMEC cells.

	IC_{50} (μM)[a]	
	HeLa	**HuMEC**
24 h	38.56 ± 3.65	> 100
48 h	15.77 ± 3.28	> 100
72 h	2.71 ± 5.53	79.53 ± 5.38

[a]Data were mean ± SD.

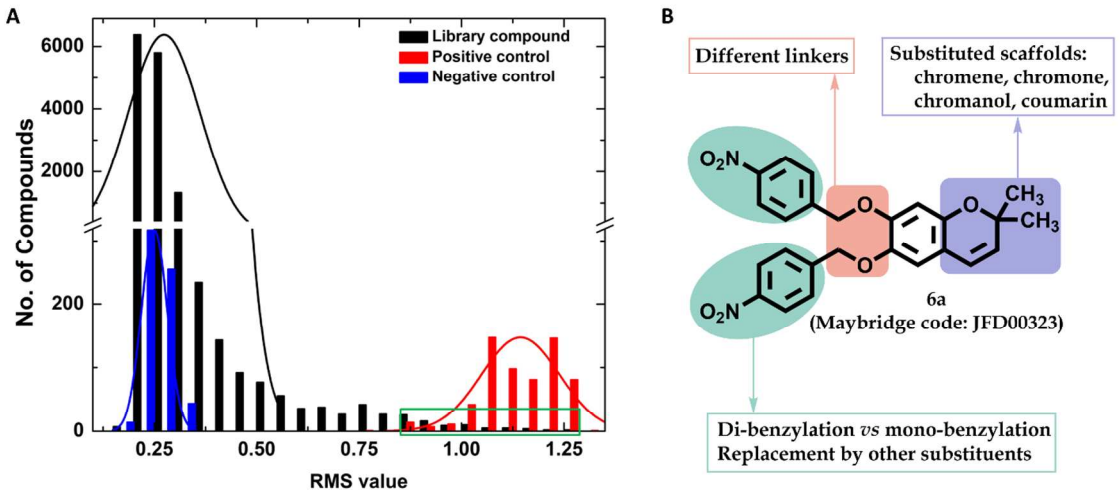

Figure 1. (A) Histogram depicting the data distribution from the HTS. A total of 14,400 compounds from the Maybridge HitFinder v11 library along with the positive control (poly I:C = 5 µg/mL) and the negative control (cells + medium + DMSO) were distributed based on the RMS values. RMS = $\sqrt{\frac{a_1^2+a_2^2}{2}}$, where a_1 and a_2 represent the duplicate set of values for positive, negative, and test controls. (B) Structure of hit **6a** from the HTS and optimization plans.

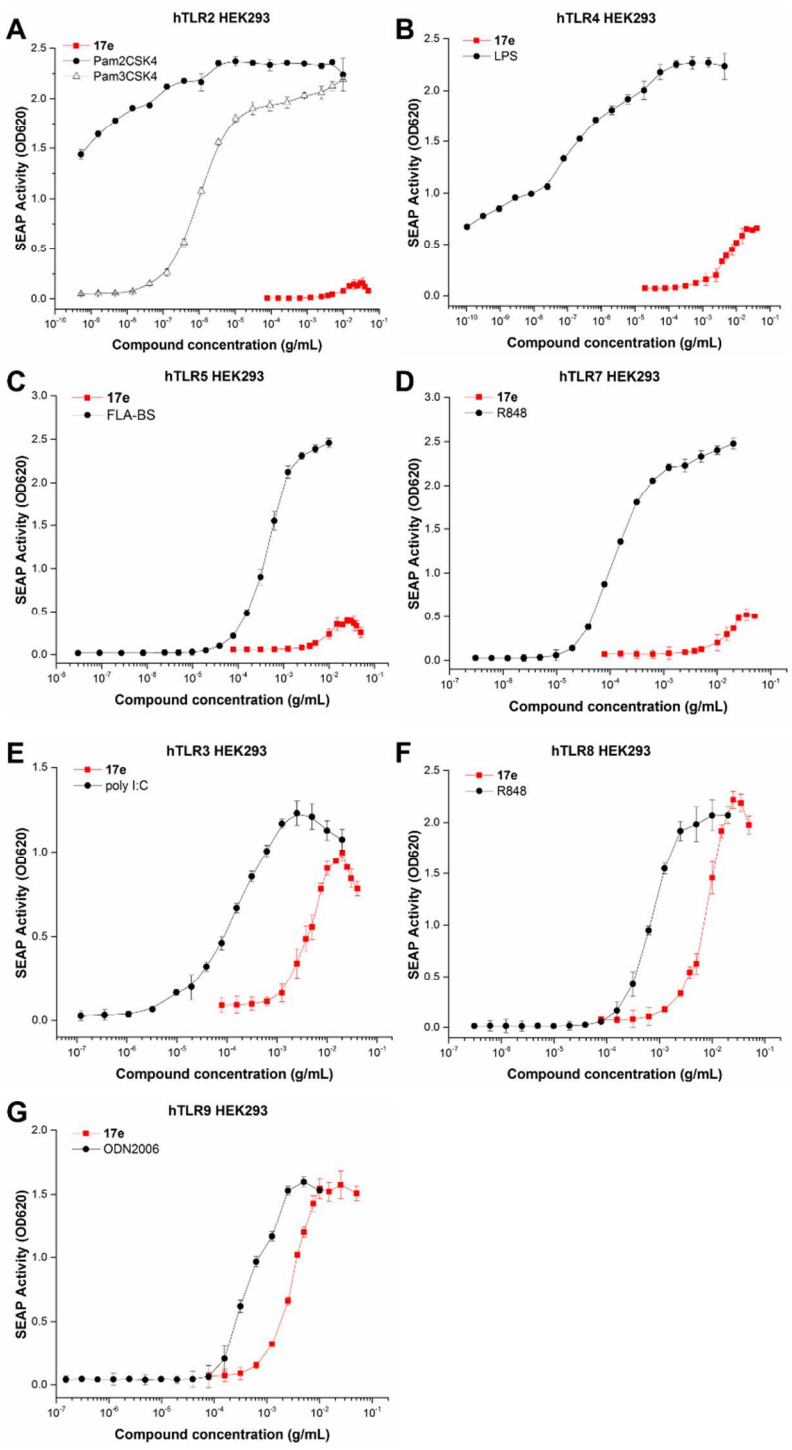

Figure 2. Effect of **17e** on NF-κB activation in human (A) TLR2, (B) TLR4, (C) TLR5, (D) TLR7, (E) TLR3, (F) TLR8, and (G) TLR9 HEK293 reporter cells by the SEAP assay. Results shown are averages of three independent experiments and error bars represent mean ± SD.

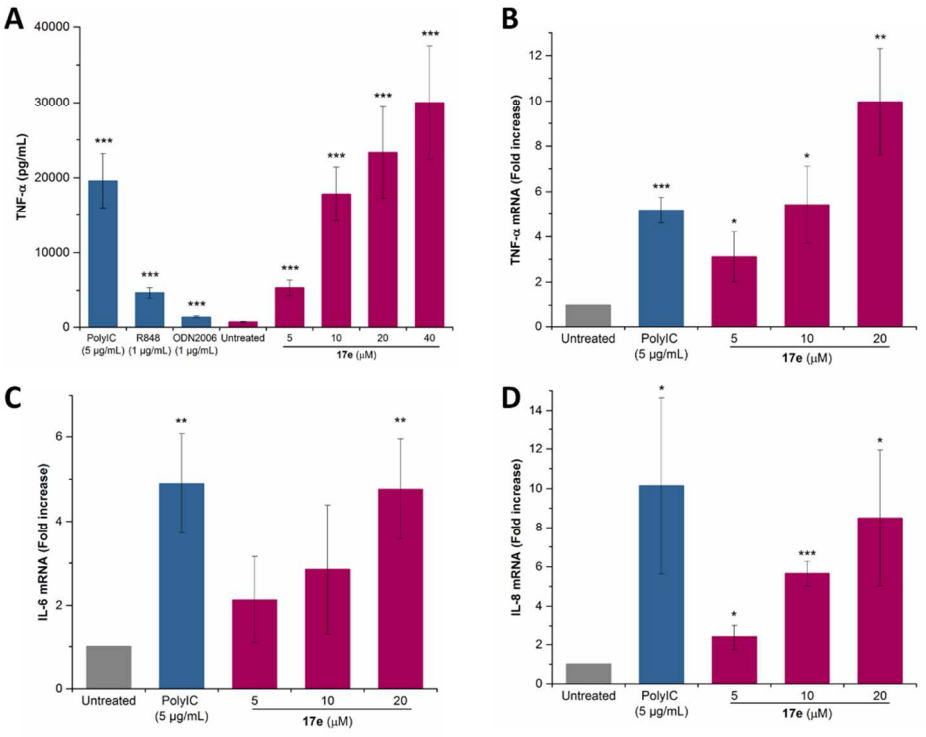

Figure 3. (A) Effect of **17e** on expression of proinflammatory cytokine TNF-α. After treatment for 24 h, TNF-α cytokine production by TLR ligands and **17e** in THP-1 cells were tested by ELISA. The mRNA profiles of (B) TNF-α, (C) IL-6, and (D) IL-8 were evaluated by qRT-PCR in THP-1 cells stimulated with poly I:C (5 μg/mL) and different concentrations of **17e** for 12 h. Each figure illustrates the mRNA fold changes compared with the untreated control set. Results shown are averages of three independent experiments and error bars represent mean ± SD. *$p < 0.05$, **$p < 0.01$, and ***$p < 0.001$ compared with the untreated group.

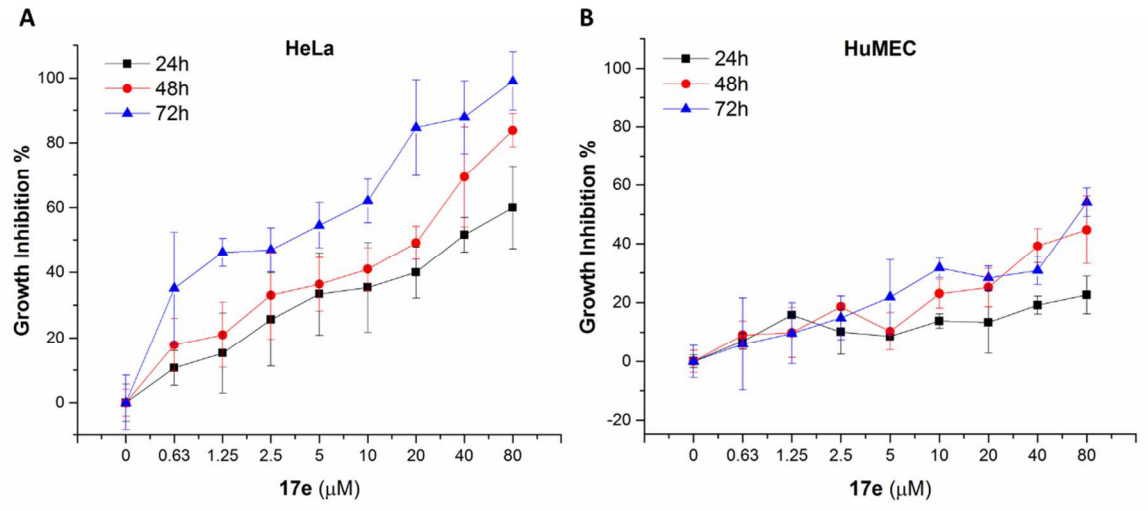

Figure 4. Effects of **17e** on growth of (A) HeLa and (B) HuMEC cells. Exponentially growing cells were treated with the designated concentrations of **17e** for the indicated durations. Cell viability was tested by measuring WST-1 absorbance at 450 nm at different time intervals. Results shown are averages of three independent experiments and error bars represent mean ± SD.

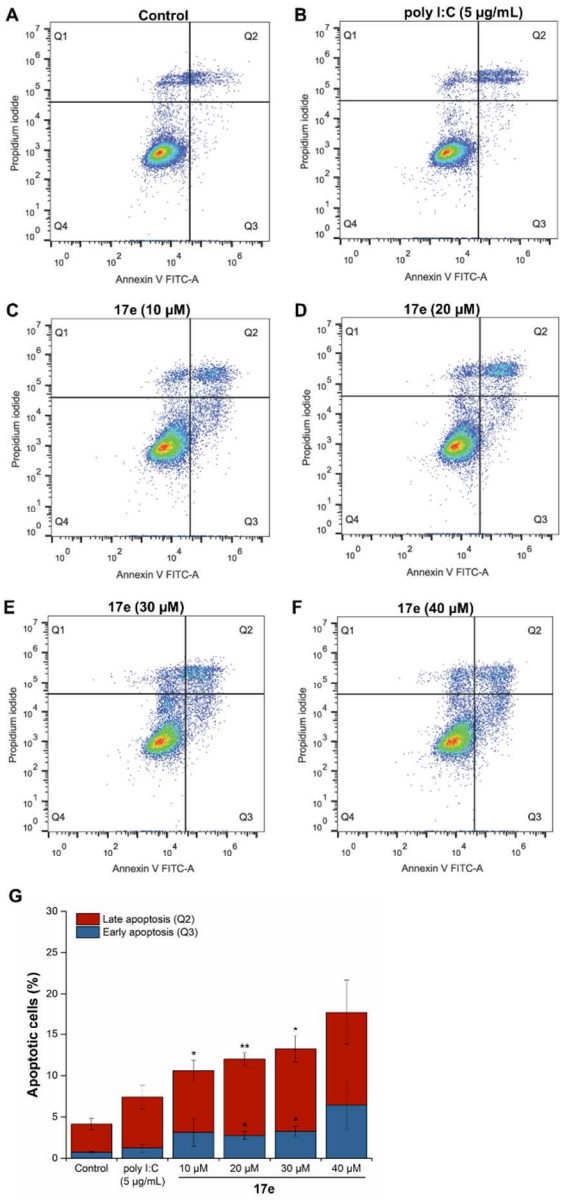

Figure 5. Effect of **17e** on induction of apoptosis. HeLa cells were treated for 24 h, and apoptosis was determined with annexin V/PI double staining and flow cytometry. (A) Control (DMSO); (B) 5 μg/mL of poly I:C; (C) 10 μM, (D) 20 μM, (E) 30 μM, and (F) 40 μM of **17e**. The cells in quadrants Q1, Q2, Q3, and Q4 signify the necrotic, late apoptotic, early apoptotic, and viable cells, respectively. Results shown are representative of three independent experiments. (G) The percentages of early and late apoptotic cells were quantitatively depicted. Results shown are averages of three independent experiments and error bars represent mean ± SD. *$p < 0.05$ and **$p < 0.01$ compared with the control group.

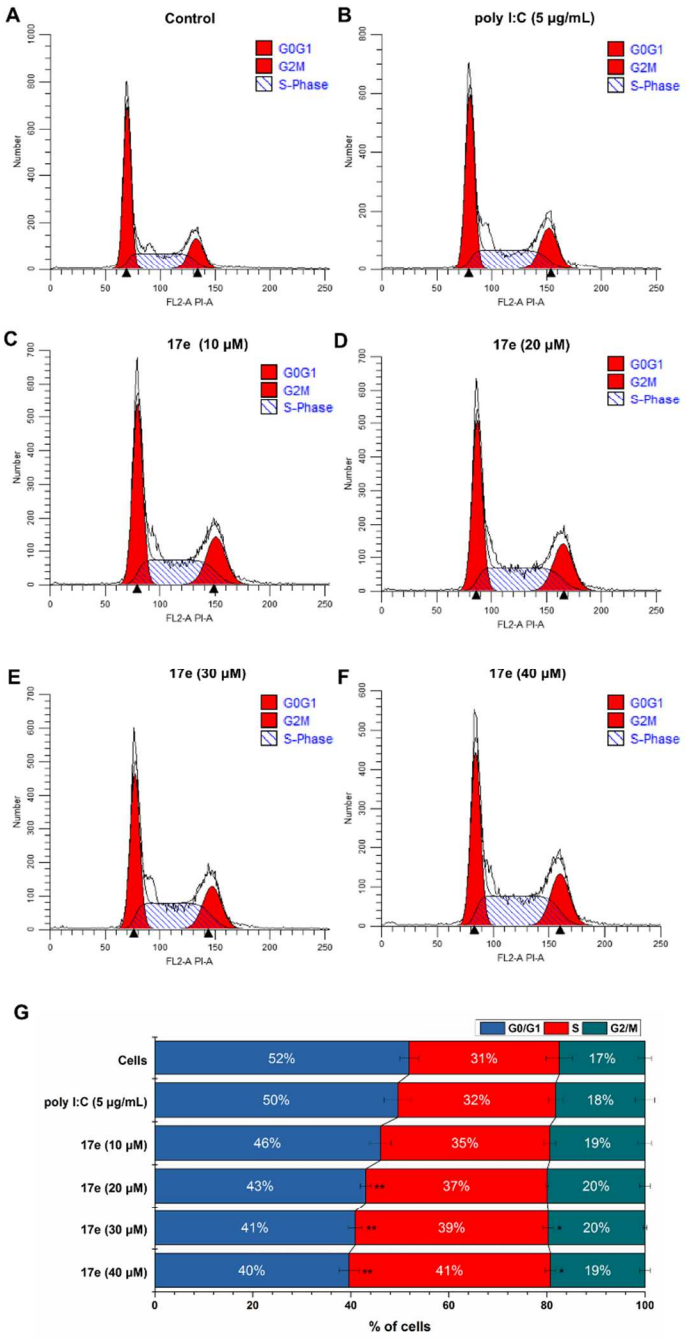

Figure 6. Effect of **17e** on cell cycle. HeLa cells were treated for 24 h and the cell cycle was detected using PI staining and flow cytometry. (A) Control (DMSO); (B) 5 µg/mL of poly I:C; (C) 10 µM, (D) 20 µM, (E) 30 µM, and (F) 40 µM of **17e**. Results shown are representative of three independent experiments. (G) The percentages of cells at each phase are quantitatively depicted. Results shown are averages of three independent experiments and error bars represent mean ± SD. *$p < 0.05$ and **$p < 0.01$ compared with the control group.

Table of Contents graphic